

UNIVERSITÄTSKLINIKUM HAMBURG-EPPENDORF

Kopf- und Neurozentrum
Klinik und Poliklinik für Neurochirurgie

Prof. Dr. med. Manfred Westphal

Zentrum für Experimentelle Medizin
Institut für Neurophysiologie und Pathophysiologie

Prof. Dr. med. Andreas K. Engel

Abnormal behavior of parkinsonian rats and genetic changes following high-frequency stimulation of the subthalamic nucleus

Dissertation

zur Erlangung des Grades eines Doktors der Medizin
an der Medizinischen Fakultät der Universität Hamburg.

vorgelegt von:

Benjamin Max Grieb
aus Mainz

Hamburg 2014

**Angenommen von der
Medizinischen Fakultät der Universität Hamburg am: 11.12.2015**

**Veröffentlicht mit Genehmigung der
Medizinischen Fakultät der Universität Hamburg.**

Prüfungsausschuss, der Vorsitzende: PD Dr. Wolfgang Hamel

Prüfungsausschuss, zweiter Gutachter: Prof. Dr. Andreas Engel

*If you don't climb the mountain
you can't see the view*

– Anonymous climber

Contents

Part A	
“Decomposition of abnormal free locomotor behavior in a rat model of Parkinson’s disease”	6
Part B	
i. “High-frequency stimulation of the subthalamic nucleus counteracts cortical expression of major histocompatibility complex genes in a rat model of Parkinson’s disease”	18
ii. Supporting information	33
Summary	37
Appendices	47

*This thesis was written in
Hamburg, Jerusalem, Aachen, Heidelberg,
Koh Yao Noi, Tonsai Beach and Serramonacesca*

Part A

**Decomposition of abnormal free locomotor behavior
in a rat model of Parkinson's disease**

Published in Frontiers in Systems Neuroscience on November 27, 2013



Decomposition of abnormal free locomotor behavior in a rat model of Parkinson's disease

Benjamin Grieb^{1,2*}, Constantin von Nicolai^{1,3}, Gerhard Engler¹, Andrew Sharott^{1,4},
Ismini Papageorgiou⁵, Wolfgang Hamel⁶, Andreas K. Engel^{1†} and Christian K. Moll^{1†}

¹ Department of Neurophysiology and Pathophysiology, University Medical Center Hamburg-Eppendorf, University of Hamburg, Hamburg, Germany

² Department of General Psychiatry, Center for Psychosocial Medicine, University of Heidelberg, Heidelberg, Germany

³ Centre for Integrative Neuroscience, University of Tübingen, Tübingen, Germany

⁴ Medical Research Council, Anatomical Neuropharmacology Unit, Department of Pharmacology, University of Oxford, Oxford, UK

⁵ Division of General Neurophysiology, Institute of Physiology and Pathophysiology, University of Heidelberg, Heidelberg, Germany

⁶ Department of Neurosurgery, University Medical Center Hamburg-Eppendorf, University of Hamburg, Hamburg, Germany

Edited by:

Hagai Bergman, The Hebrew University, Israel

Reviewed by:

M. Gustavo Murer, Universidad de Buenos Aires, Argentina

Nicola B. Mercuri, University of Rome, Italy

*Correspondence:

Benjamin Grieb, Department of General Psychiatry, Center for Psychosocial Medicine, University of Heidelberg, Voßstrasse 2, 69115 Heidelberg, Germany
e-mail: benjamin.grieb@med.uni-heidelberg.de

† These authors have contributed equally to this work.

Poverty of spontaneous movement, slowed execution and reduced amplitudes of movement (akinesia, brady- and hypokinesia) are cardinal motor manifestations of Parkinson's disease that can be modeled in experimental animals by brain lesions affecting midbrain dopaminergic neurons. Most behavioral investigations in experimental parkinsonism have employed short-term observation windows to assess motor impairments. We postulated that an analysis of longer-term free exploratory behavior could provide further insights into the complex fine structure of altered locomotor activity in parkinsonian animals. To this end, we video-monitored 23 hours of free locomotor behavior and extracted several behavioral measures before and after the expression of a severe parkinsonian phenotype following bilateral 6-hydroxydopamine (6-OHDA) lesions of the rat dopaminergic substantia nigra. Unbiased stereological cell counting verified the degree of midbrain tyrosine hydroxylase positive cell loss in the substantia nigra and ventral tegmental area. In line with previous reports, overall covered distance and maximal motion speed of lesioned animals were found to be significantly reduced compared to controls. Before lesion surgery, exploratory rat behavior exhibited a bimodal distribution of maximal speed values obtained for single movement episodes, corresponding to a "first" and "second gear" of motion. 6-OHDA injections significantly reduced the incidence of second gear motion episodes and also resulted in an abnormal prolongation of these fast motion events. Likewise, the spatial spread of such episodes was increased in 6-OHDA rats. The increase in curvature of motion tracks was increased in both lesioned and control animals. We conclude that the discrimination of distinct modes of motion by statistical decomposition of longer-term spontaneous locomotion provides useful insights into the fine structure of fluctuating motor functions in a rat analog of Parkinson's disease.

Keywords: 6-OHDA lesions, stereology, spontaneous activity, Parkinson disease, video monitoring

INTRODUCTION

Neurotoxin-induced degeneration of nigral dopamine neurons in experimental animals results in motor abnormalities relevant to motor symptoms of Parkinson's disease (PD; Cenci et al., 2002). One strategy to deplete midbrain dopaminergic neurons in rats is to infuse the neurotoxin 6-hydroxydopamine (6-OHDA) directly into the substantia nigra pars compacta (SNc; Schwarting and Huston, 1996a,b), which can also cause moderate cell death in the neighboring ventral tegmental area (VTA). In the prototypic toxin-induced rat model of PD, unilateral intracerebral 6-OHDA injections lead to the expression of a strictly lateralized hemiparkinsonian phenotype, the behavioral sequelae of which have been described in great detail. A wide variety of different behavioral tests are used to examine motor changes associated with the asymmetrical depletion of the nigrostriatal dopaminergic system, e.g., skilled motor tasks (Mokry et al., 1995; Truong et al., 2006), footprint-analysis (Metz et al., 2005),

treadmill running (Brazhnik et al., 2012), or drug-induced rotation (Ungerstedt, 1971; Kelly, 1975). Compared to the unilateral 6-OHDA model, bilaterally lesioned rats have been used less commonly, although they display a far more severe parkinsonian phenotype. In this respect, the slowness and scarcity of movement observed in the bilateral 6-OHDA rat model resembles more closely the marked expression of PD-like symptoms in monkeys treated systemically with 1-methyl-4-phenyl-1,2,3,6-tetrahydropyridine (Bergman et al., 1990) and cardinal motor manifestations of human PD patients in advanced disease stages. The development of pronounced motor impairment in rats with severe bilateral 6-OHDA lesions is, however, often accompanied by aphagia, adipsia and abulia (Schallert et al., 1978; Sakai and Gash, 1994; Cass et al., 2005; Ferro et al., 2005).

Rat equivalents of akinesia are commonly assessed in an "open-field" environment. Most often, rat motion (including scanning, walking or running, as well as rearing) is detected by

consecutively breaking light beams arranged in an array around the arena (Cass et al., 2005; Ferro et al., 2005; Belujon et al., 2007). Other methods to quantify locomotor capacities are wheel (Schallert et al., 1978) or treadmill running (Avila et al., 2010). These standard measurements usually assess a short period of 10–60 min of locomotor activity (Cass et al., 2005; Ferro et al., 2005; Belujon et al., 2007), assuming a stable motor phenotype over time. However, these methods may underestimate the complexity of exploratory behavior, in particular long-term motor fluctuations.

Recently, a novel analytical approach to video-based tracking data utilized the statistical discrimination of rat motor behavior on the basis of speeds (Drai et al., 2000; Drai and Golani, 2001). This form of data analysis showed that naïve rats, but also naïve mice (Drai et al., 2001), use distinctly different modes of motion to explore their environment. The current study aimed to assess the impact of dopamine depletion on these naturally occurring behavioral patterns. We hypothesized that expression of a severe parkinsonian phenotype would not only reduce overall motion speed, as could be assessed with other standard quantification methods, but would also alter the fine spatio-temporal structure of exploratory locomotion modes. To test this, we adapted the analysis approach of Drai and colleagues to video-based tracking data from 23 hours of continuous and spontaneous locomotion of bilaterally 6-OHDA lesioned and control rats.

MATERIALS AND METHODS

ANIMALS

Animal experiments were approved by the local government authorities of Hamburg and carried out in accordance with the European Council Directive 86/609/EEC. All experiments were performed on male Brown Norway rats (*Rattus norvegicus*; Charles River Laboratories, Sulzfeld, Germany). All efforts were made to minimize suffering. The bilateral 6-OHDA lesion model is known to be associated with high mortality due to aphagia/adipsia and following loss of body weight (Ferro et al., 2005). Careful clinical inspection and weighting of animals was performed on a daily basis. In general, we offered a soft and moist rat chow and 10%-glucose solution in addition to standard chow and water *ad libitum*. To sustain aphagic and adipsic PD rats, we administered a liquid and high caloric nutrition for rodents (Altromin, Lage, Germany) by manual needle feeding. In total, the dropout rate was 5/14 PD rats. Dropouts included perioperative death ($n = 2$ PD) and loss of $>20\%$ body weight without stabilization of weight loss within 14 days after surgery ($n = 3$ PD) which led to euthanasia of these animals by decapitation under deep anesthesia (i.p.-injection of ketamine 100 mg/kg, xylazine 6 mg/kg).

EXPERIMENTAL DESIGN

We randomly assigned 14 rats to a PD group receiving bilateral 6-OHDA injections into the SNc and eight rats to a control group receiving bilateral vehicle injections (preoperative weight: 384 ± 32 g, mean \pm SD). Video tracking of 23 hours of spontaneous locomotor activity was performed prior to surgery. Due to the labor intensity of sustaining PD rats we ran the experiment in two phases. Within the first subset of 10 rats ($n = 8$ PD; $n = 2$

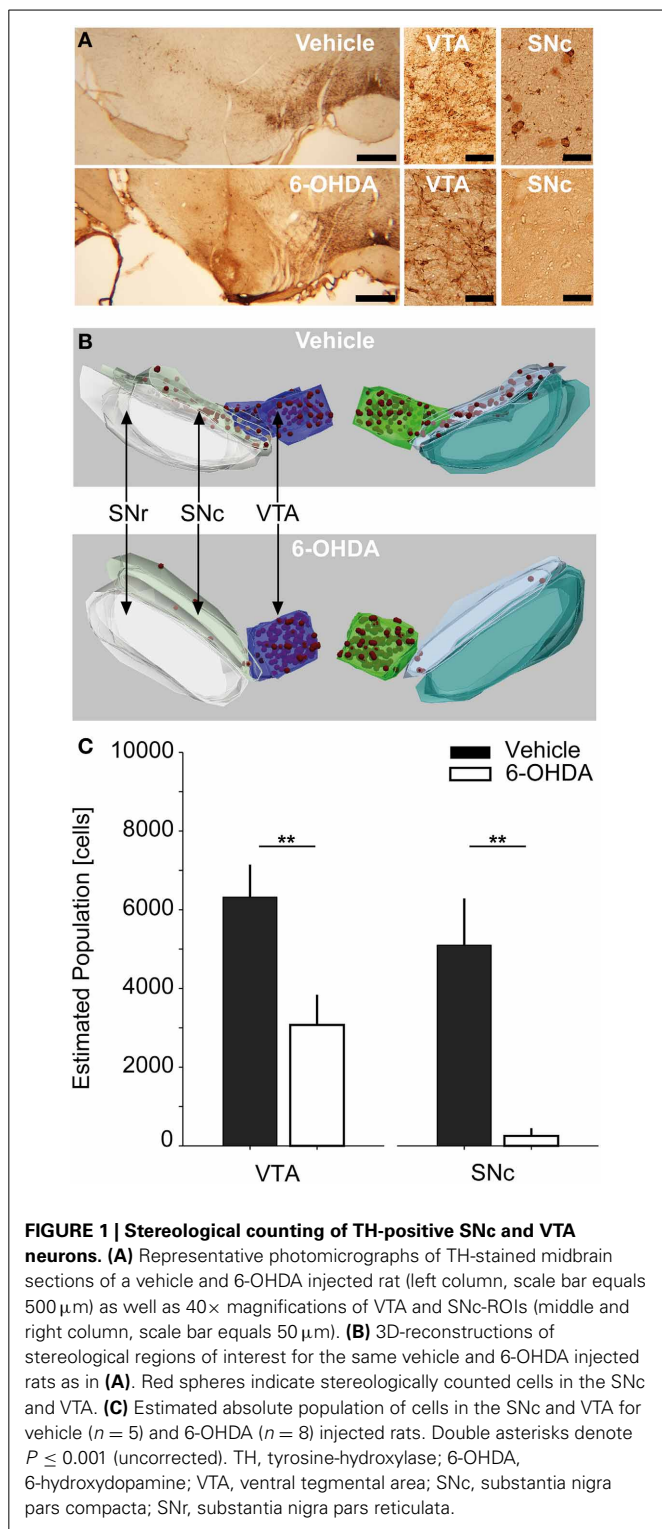
controls) the dropout rate was 4/8 PD rats. The second subset of 12 rats ($n = 6$ PD; $n = 6$ controls) exhibited a dropout rate of 1/6 PD rats. Postoperative locomotor activity was assessed after a recovery period of 12 ± 2 days in the first subset and 28 ± 2 days in the second subset. After postoperative video monitoring, all rats were subsequently used in a separate study. We sacrificed rats after induction of deep anesthesia (ketamine/xylazine) ~ 14 weeks after lesioning by transcardial perfusion with saline. A midbrain tissue block was immersion-fixed in 4%-PFA-solution (paraformaldehyde in 0.1 M phosphate buffered saline, Sigma-Aldrich) for subsequent histological TH-staining and stereological counting of tyrosine hydroxylase (TH)-positive SNc and VTA neurons.

BILATERAL 6-HYDROXYDOPAMINE LESIONS

Stereotactic injections were performed under general anesthesia introduced with isoflurane (Baxter Germany GmbH, Unterschleißheim, Germany) and maintained with i.p.-injections of ketamine (65 mg/kg, Dr. E. Gräub AG, Bern, Switzerland) and xylazine (3 mg/kg, Bayer Health Care, Leverkusen, Germany). Thirty minutes prior to 6-OHDA or vehicle injections, rats received a bolus i.p.-injection of desipramine (25 mg/kg, Sigma-Aldrich, Munich, Germany) to minimize uptake of 6-OHDA in noradrenergic midbrain neurons (Schwartz and Huston, 1996b). Cardiopulmonary protection was assured by an initial bolus injection of atropine (0.25 mg/kg, B. Braun Melsungen AG, Melsungen, Germany). Body temperature was monitored during surgery with a rectal probe and hypothermia was prevented with an adjustable heating pad (FST, Heidelberg, Germany). In addition, the eyes were covered with dexpanthenol cream to prevent exsiccation. Animals were mounted in a stereotactic frame (David Kopf Instruments, Tujunga, USA). To target the SNc a Hamilton microliter-syringe (FST) was lowered through a burr hole placed at +4 mm AP and ± 2.2 mm ML using the interaural line as reference (Paxinos and Watson, 2005). The syringe was slowly lowered to the target depth at -8 mm relative to the dura. Five microliter neurotoxin ($3 \mu\text{g}/\mu\text{l}$ 6-OHDA hydrochloride free base in 0.2% ascorbic acid solution, stored on ice; Sigma-Aldrich) or vehicle (aqua injectabilia, 0.2% ascorbic acid solution; Sigma-Aldrich) was slowly infused at a rate of $0.5 \mu\text{l}/\text{min}$ and the syringe was left in place for 2 min to allow for complete absorption of the toxin. The burr hole was closed with bone wax and the procedure was repeated in the contralateral hemisphere. Rats received s.c.-injections of metamizole (100 mg/kg, Medistar, Holzwickede, Germany) for postoperative analgesia following surgery and on behavioral signs of pain distress.

STEREOLOGY

To count TH-positive dopaminergic cells in PD rats and controls we performed free-floating TH-immunohistochemistry on serial $40 \mu\text{m}$ coronal sections of the midbrain. **Figure 1A** displays representative examples of photomicrographs depicting TH-stained midbrain sections from a vehicle and 6-OHDA injected rat. Due to technical reasons we could only obtain stereology in a subset of 8/9 PD-rats and 5/8 controls. PFA-fixed tissue blocks containing SNc and VTA were transferred to 30%-sucrose solution and kept at 4°C for 24 hours. Sections were cut with a freezing-microtome



(Leica Instruments, Wetzlar, Germany) and stained in free-floating fashion for TH-activity. Briefly, sections were washed in phosphate buffer (0.01 M PBS, Sigma-Aldrich), incubated with 3% H_2O_2 -solution for 3 min to block endogenous peroxidase activity and incubated with 2% normal horse serum (added with

0.3% Triton X-100, Sigma-Aldrich) for 30 min. Sections were then incubated over night at 4°C with the primary TH-antibody (1:250, monoclonal mouse antibody, Novocastra reagents, Leica Microsystems, Wetzlar, Germany), followed by the biotinylated secondary antibody (1:400, Novocastra reagents) for 30 min, and afterwards incubated with avidin and biotinylated horseradish peroxidase (ABC kit, Novocastra reagents) for another 30 min. TH was visualized by adding peroxidase substrate (0.02% DAB reagent in 0.003% H_2O_2 in PBS) for 2–10 min duration. Finally, sections were mounted on glass slides, dehydrated in an increasing alcohol row and fixed under a cover slid with Roti Histokitt II (Carl Roth, Karlsruhe, Germany).

Unbiased stereological counting of TH-positive cells in the SNc and VTA was performed using the Stereoinvestigator Software (Version 10.0, MicroBrightField Inc., Williston, Vermont, USA). The hardware consisted of an Olympus Bx61 brightfield microscope (Olympus Deutschland GmbH, Hamburg, Germany) equipped with a Microfire TM A/R camera (Optronics, California, USA) and an x-y-z galvano table (Carl Zeiss AG, Jena, Germany). The optical fractionator probe (West et al., 1991; West, 2002) was applied on series of 40 μm thick coronal sections. To assure sampling of comparable structural parts, the stereological analysis was centered on an independent anatomical hallmark (the rootlets of the oculomotor cranial nerve). Overall we sampled 10 sections (sampling rate of 1.2 ± 0.3 mean \pm SD sections) spanning $\sim 480 \mu\text{m}$ in the cranio-caudal dimension. However, due to availability of continuous TH-sections containing SNc and VTA, three rats were investigated using 7, 8, or 9 sections, respectively. Using a 2.5 \times magnification with numerical aperture of 0.075 we defined three anatomical regions of interest (ROI), i.e., the SNc, the VTA and the substantia nigra pars reticulata (SNr) (Paxinos and Watson, 2005). For examples of anatomical 3-D reconstructions of ROIs and counted cells, see Figure 1B. Cell counting was performed using a 40 \times Plan-Neofluar dry type objective lens with a numerical aperture of 0.75 (Carl Zeiss AG) within the SNc and VTA-ROIs. The counting frame (50 \times 50 μm) with dissector height of 20 μm was applied with a uniform random sampling grid of 150 \times 150 μm (optical dissector volume of 50,000 μm^3 , sampling grid area of 22,500 μm^2 , Gundersen, 1986). Schaeffer's estimated coefficient of error ranged between 0.05 and 0.12 for the VTA of both controls and PD animals, as well as the SNc of controls. For SNc-ROIs of PD animals it ranged between 0.3 and 0.9, reflecting the scarceness of TH-positive cells in this area (Gundersen, 1986; West, 2002). The total volume of the sampled SNc and VTA parts was stereologically estimated using the Cavalieri method (Gundersen and Jensen, 1987). Our histological regime resulted in robust sampling >200 neurons per VTA and SNc in vehicle injected controls, enabling us to express TH-positive cell numbers in absolute numbers. Cell counts were calculated separately for each ROI and hemisphere, respectively, and combined across hemispheres ($n = 6$ hemispheres per group).

To assess the symmetry of depletion we calculated the laterality index (LI) for each rat (Seghier, 2008), $LI = f \times (E_{LH} - E_{RH}) / (E_{LH} + E_{RH})$, where E_{LH} and E_{RH} are the combined VTA and SNc estimates of TH-positive cells for the left and right

hemisphere, respectively, and f is a scaling factor set to 1 resulting in the LI to be bound between -1 and 1 .

BEHAVIORAL MONITORING

Locomotion of 6-OHDA or vehicle injected rats was investigated via continuous video monitoring of 23 hours of spontaneous behavior in an open field-like environment. We used an infrared video-based tracking system (VideoMot 2.0, TSE Systems, Bad Homburg, Germany) to record movement paths as time series of x-y-positions at a sampling rate of 12.8 Hz. The recording arena was spaced 70×100 cm with 40 cm high walls (i.e., 320×435 pixel after frame grabbing and offline analysis) and equipped with three food pellet feeders and one water outlet positioned in the corners. The ground was covered with bedding. The arena size was chosen to be ~ 3 times larger than the size of the rat's home cage to allow for generation of more naturalistic movement patterns including running. The arena was placed in a custom-made recording box lined with foamed plastic to ensure light and acoustic insulation. Recordings took place under constant darkness.

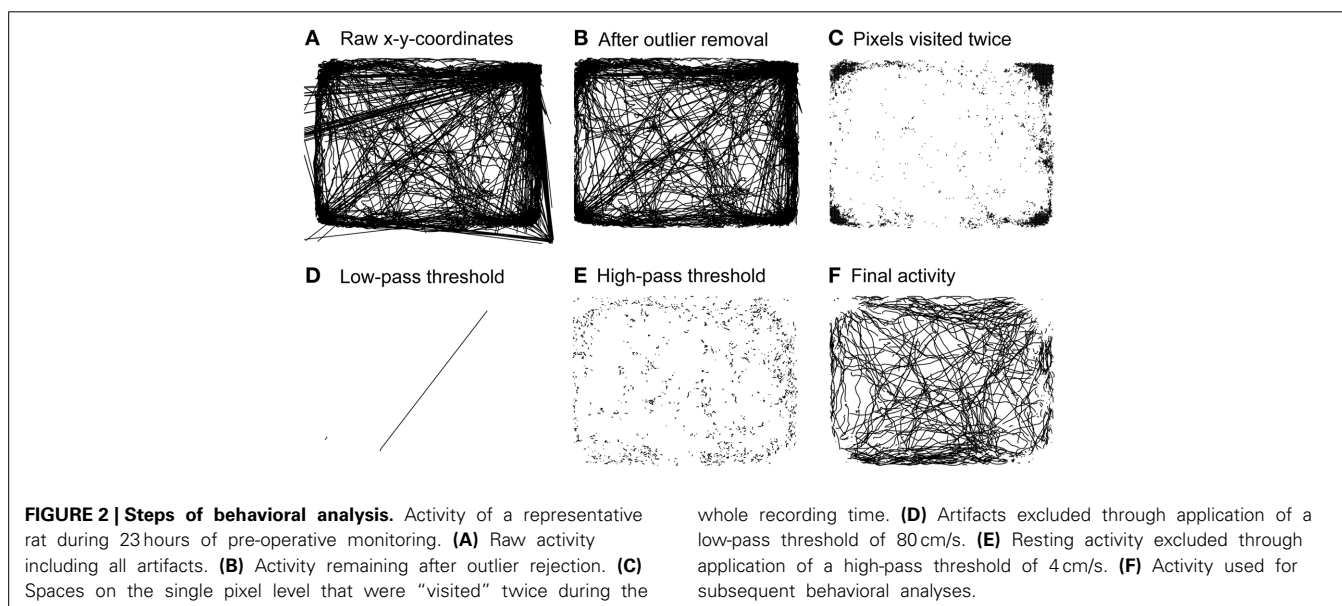
BEHAVIORAL DATA ANALYSIS

To analyze spontaneous long-term behavior we modified a data processing and analysis approach developed for open-field locomotion in rodents (Drai et al., 2000; Drai and Golani, 2001). All routines were written in MATLAB (The Mathworks, Natick, USA). The analytical approach is based on the idea of calculating single speed values (cm/s) from x-y-position time series using a sliding window, separating rest vs. motion episodes and characterizing motion episodes by the maximal speed reached within each episode rather than the average speed of a given episode. Our modified analysis consisted of five separate analysis steps (see **Figure 2**): First, raw x-y-position time series data obtained for 23 hours at a sampling rate of 12.8 Hz ($\sim 1,000,000$ single data points) contained large amounts of artifacts (see **Figure 2A**). Typically, artifacts resulted from spurious "jumping" within a

continuous x-y-position time series to distant places and back. Frequent sources of artifacts lay outside the actual recording arena and could therefore be removed through spatial outlier rejection. However, artifacts also appeared within the arena, generally jumping toward the arena's corners where animals spent most of their resting time (**Figure 2B**). All places on the pixel level that were "visited" twice during the recording time were neglected, eliminating artifacts associated with resting spots (**Figure 2C**). To further de-noise the recordings we applied a low-pass threshold of 80 cm/s (**Figure 2D**), as preliminary data screening showed that no rat reached speed levels >70 cm/s inside the recording arena (data not shown). Single speed values were calculated on position time series with a moving window of 0.3 s (Drai et al., 2000; Drai and Golani, 2001). Separation of resting vs. motion episodes was done by high-pass thresholding speed values at a noise level of 4 cm/s (**Figure 2E**). This threshold was based on previous work of Drai et al. (2000) and adapted to the distribution of single speeds in our data set with a peak at 4 cm/s (data not shown). The remaining motion episodes were used for further analysis (**Figure 2F**). To compensate for erroneous separation of movement episodes resulting from artifact correction we interpolated x-y-coordinates of single missing values.

BEHAVIORAL ENDPOINTS

Smoothed histograms of log transformed maximal speed values, termed "log max-SD," were used to identify different modes of motion in control and PD rats (Drai et al., 2000; Drai and Golani, 2001). A Gaussian mixture model was fitted toward the empirical data to obtain information about the localization of different "gears" of motion within the distribution of speeds. Gears were separated at 10 cm/s, a value consistently derived from preoperative recordings. Descriptive locomotion parameters were calculated for slow (i.e., first gear) and fast (i.e., second gear) episodes. However, as the dissection of second gear episodes allowed a view on full-blown motion, we concentrated our analysis on such episodes.



The six different behavioral endpoints were defined as: (1) incidence of fast speed movement episodes, which is the percentage of second gear episodes relative to the number of all motion episodes; (2) absolute distance, calculated as the cumulative sum of the overall covered distance for all motion episodes; (3) average maximal movement speed, corresponding to the mean of all maximal speeds of second gear episodes; (4) dwell time, i.e., the average time it took the rats to execute a motion episode; (5) spatial spread, i.e., the mean distance covered within a motion episode; (6) curvature of movement tracks, i.e., the ratio of the detected real motion track distance and the distance of the virtual line connecting two coordinate pairs directly during temporal windows of 0.5 s. Curvatures were averaged across all windows of a given motion episode.

Our experimental paradigm allowed for *post-hoc* splitting of the experimental groups into rats monitored after 12 ± 2 days and 28 ± 2 days weeks of recovery. We separately analyzed the correlation between the six behavioral endpoints and the estimated absolute population of TH-positive neurons in the SNc and VTA, the corresponding LI of cell depletion and the observed weight reduction for the 6-OHDA and vehicle injected control group. We utilized bootstrap regressions, which do not rely on a normal distribution of data.

STATISTICAL ANALYSIS

All *post-hoc* analyses were performed using the MATLAB Statistics Toolbox and the BRAVO Toolbox for Bootstrap Regression Analysis of Voxelwise Observations. In case of non-normal data distributions, we employed non-parametric statistical testing (Wilcoxon rank sum test). An alpha level of 0.05 was used for all statistical tests. All statistical results are given as mean \pm standard deviation (SD). We corrected *P*-values for multiple comparisons using the false discovery rate (FDR) method (Benjamini and Hochberg, 1995) in case of descriptive behavioral results and multiple bootstrap regression analyses. Bootstrap regressions were performed with 5000 iterations. For descriptive analysis of behavioral endpoints alone, *P*-values were FDR-corrected for a total of 48 different comparisons (2 experimental groups, 6 behavioral endpoints; 4 different comparisons: preoperative vs. 12 + 28 days postoperative, preoperative vs. 12 days postoperative, preoperative vs. 28 days postoperative and 12 days postoperative vs. 28 days postoperative). For bootstrap regressions, *P*-values were FDR-corrected for a total of 55 regressions (the estimated neuronal population of the SNc and VTA, the LI, weight reduction and 6 behavioral endpoints).

RESULTS

STEREOLOGICAL COUNTING OF TH-POSITIVE SNc AND VTA NEURONS

Bilateral injections of $15 \mu\text{g}$ 6-OHDA into the SNc resulted in extensive cell death of dopaminergic neurons in the SNc and intermediate cell death in the VTA (Figure 1C). The estimated population of TH-positive neurons for combined SNc-ROIs was reduced by -95% in PD rats compared to controls. The absolute number of cells within combined SNc-ROIs was 253.8 ± 196.9 in PD vs. 5098 ± 1189 in control rats ($P = 0.001$). For combined VTA-ROIs, the estimated population of TH-positive neurons was reduced by -51.4% in PD rats compared to controls. Here, the

absolute number of cells within combined VTA-ROIs was 3073 ± 766 in PD vs. 6318 ± 828 in control rats ($P = 0.001$). We also tested whether the cell estimates differed significantly between the two subgroups that were monitored 12 and 28 days after lesioning. No statistically significant difference was found for either VTA or SNc-ROIs of 6-OHDA or vehicle injected rats (*P*-values > 0.25 , data not shown). Furthermore, the estimated populations within single ROIs did not differ significantly between left vs. right hemispheres in PD and control rats, respectively ($P > 0.2$). Likewise, the LI for 6-OHDA treated rats was 0.14 ± 0.2 and 0.08 ± 0.01 for controls ($P = 1$, data not shown).

POSTSURGICAL COURSE

Careful daily inspection of PD and control rats in the home cage environment revealed reduced spontaneous locomotion and movement speed of 6-OHDA-treated rats. Body posture appeared with a hunchback-like shape and hind limb rigidity was detectable upon manual assessment. PD rats displayed aphagia and adipsia leading to a reduction in body weight of $19 \pm 7.7\%$ of the preoperative weight in PD and $1.5 \pm 4.5\%$ in control rats prior to postoperative behavioral monitoring ($P = 0.002$). Three PD rats were euthanized, as they did not exhibit stabilization of weight loss within 12 days after surgery. None of the control rats showed overt movement deficits, aphagia, or adipsia. No additional signs of altered behavior that could indicate persistent pain distress were detected during inspections.

CIRCADIAN ACTIVITY

Free locomotion monitoring took place under constant dark conditions for at least 23 continuous hours. Although no external light cues were given we saw a pattern of locomotor activity reflecting a circadian rhythm in preoperative (data not shown) and postlesion recordings in vehicle injected controls (Figure 3A). In most rats we found two activity phases that were separated by a phase of reduced activity lasting ~ 12 hours each.

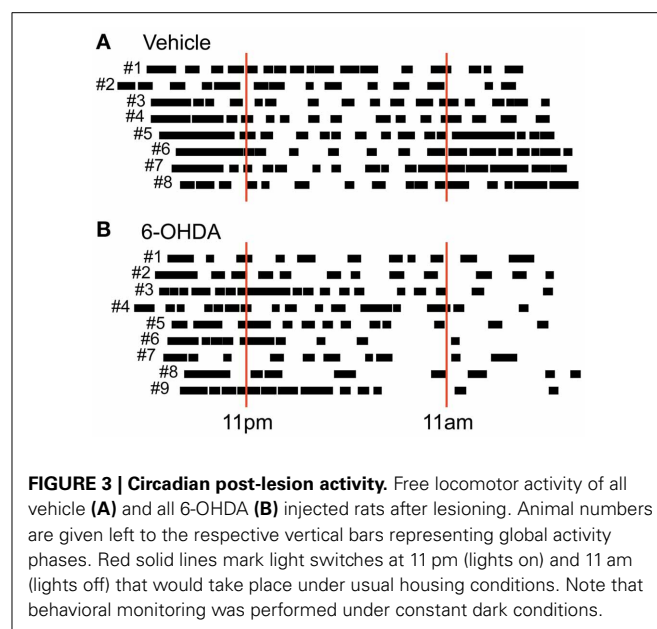


FIGURE 3 | Circadian post-lesion activity. Free locomotor activity of all vehicle (A) and all 6-OHDA (B) injected rats after lesioning. Animal numbers are given left to the respective vertical bars representing global activity phases. Red solid lines mark light switches at 11 pm (lights on) and 11 am (lights off) that would take place under usual housing conditions. Note that behavioral monitoring was performed under constant dark conditions.

This corresponds to the fact that our rats were accustomed to a 12 hour day/night cycle switching at 11 am (lights off) and 11 pm (lights on). Experiments were usually started between 5 and 6 pm and held under constant dark conditions. In PD rats, however, we found a partially disturbed circadian rhythm (**Figure 3B**) with two major changes. First, PD rats tended to show a prolonged initial global activity period and less distinguishable transition periods. Second, PD rats did not exhibit a clear rebound of activity in the later phase of monitoring.

BIMODAL DISTRIBUTION OF MAXIMAL SPEED VALUES

In prelesion recordings, characterization of movement episodes by the log max-SD resulted in a bimodal distribution (**Figure 4**). In order to distinguish between distinct gears of motion, we fitted a Gaussian mixture model to the empirical distribution of each recording. First gear speeds were centered at a log max-SD of 0.72 ± 0.02 in control and 0.71 ± 0.03 in PD rats, corresponding to a velocity of 5.1 cm/s. Second gear speeds were centered at a log max-SD of 1.24 ± 0.1 in control and 1.24 ± 0.06 in PD rats, i.e., 17.4 cm/s. Notably, 6-OHDA injections resulted in marked changes of the distribution of log max-SD values. We observed a partial loss of the bimodal distribution and curve flattening at the center of preoperative second gear episodes. This complicated the fitting of Gaussians and produced spurious results in several animals, e.g., PD rats #1, #2, and #5. Therefore, we separated gears at a log max-SD of 1 (10 cm/s), a value derived from the consistent bimodal distributions of preoperative monitoring.

INCIDENCE OF FAST SPEED MOVEMENT EPISODES

Comparing the number of first gear and second gear episodes per recording, we saw a shift in their incidence after 6-OHDA lesioning (**Figure 5A**). In the PD group, the incidence of second gear episodes decreased from $50.6 \pm 4.1\%$ to $36.4 \pm 9\%$ (pre- vs. 12 + 28 days postoperatively, $P = 0.01$, corrected). In vehicle injected controls the proportion of first gear and second gear episodes remained the same ($51.8 \pm 6.1\%$ vs. $47.4 \pm 4.7\%$, pre- vs. 12 + 28 days postoperatively, $P = 0.26$, corrected). Considering the two subpopulations separately, we only saw a significant difference after 12 days of recovery in PD rats ($P = 0.02$ at 12 days vs. $P = 0.08$ at 28 days; $P = 0.35$ for 12 vs. 28 days; corrected).

OVERALL COVERED DISTANCE

6-OHDA injections led to a reduction of the total covered distance within 23 hours of spontaneous locomotion (PD rats: 129.9 ± 25.8 m vs. 94.3 ± 28.7 m, pre- vs. 12 + 28 days postoperatively, $P = 0.05$; control rats: 143.2 ± 38 m vs. 138.9 ± 31.7 m, pre- vs. 12 + 28 days postoperatively, $P = 1$, corrected; **Figure 5B**). Again, this difference was significant for the PD group at 12 days, but not at 28 days of recovery ($P = 0.02$ at 12 days vs. $P = 0.35$ at 28 days; $P = 1$ for 12 vs. 28 days; corrected).

AVERAGE MAXIMAL MOVEMENT SPEED

The log max-SD across all second gear episodes of full motion was significantly reduced in PD rats (19.9 ± 1.7 cm/s vs. 17 ± 2 cm/s, pre- vs. 12 + 28 days postoperatively, $P = 0.02$; control rats: 20.6 ± 1.8 cm/s vs. 20 ± 1.3 cm/s, pre- vs. 12 + 28 days postoperatively, $P = 1$, corrected; **Figure 5C**). Likewise, the difference

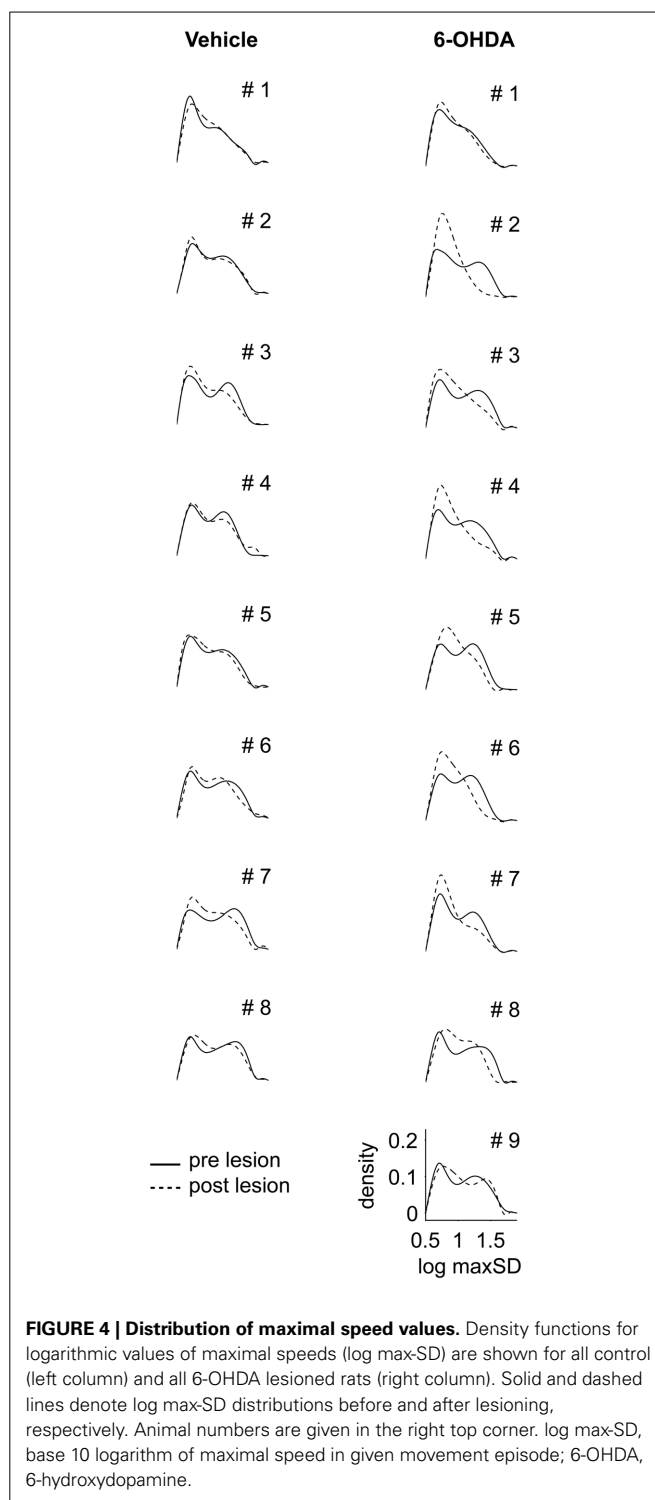


FIGURE 4 | Distribution of maximal speed values. Density functions for logarithmic values of maximal speeds (log max-SD) are shown for all control (left column) and all 6-OHDA lesioned rats (right column). Solid and dashed lines denote log max-SD distributions before and after lesioning, respectively. Animal numbers are given in the right top corner. log max-SD, base 10 logarithm of maximal speed in given movement episode; 6-OHDA, 6-hydroxydopamine.

was significant also within the PD group at 12 days of recovery ($P = 0.02$ at 12 days vs. $P = 0.18$ at 28 days; $P = 0.92$ for 12 vs. 28 days; corrected). We found no significant difference for first gear episodes ($P = 0.07$ pre- vs. 12 + 28 days postoperatively, $P = 0.25$ at 12 days, $P = 0.09$ at 28 days; $P = 0.26$ for 12 vs. 28 days; corrected).

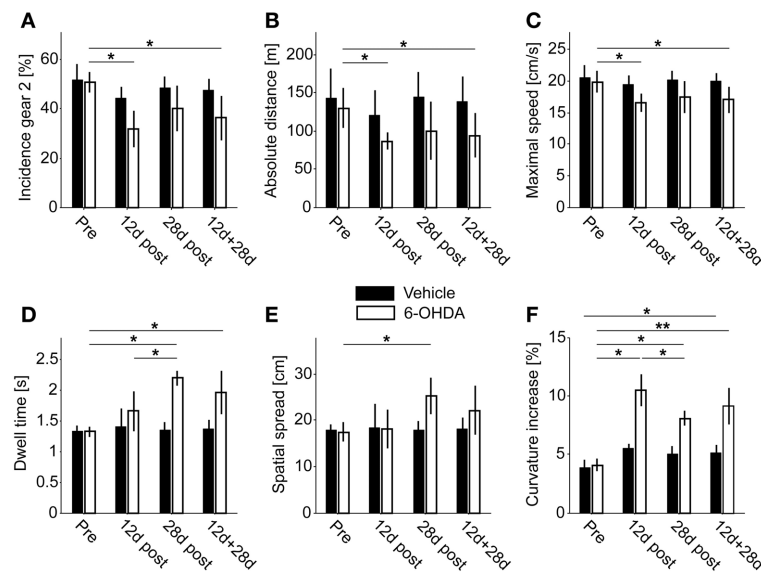


FIGURE 5 | Behavioral endpoints. (A) Incidence of second gear episodes. **(B)** Absolute covered distance. **(C)** Average maximal movement speed of second gear episodes. **(D)** Dwell time of second gear episodes. **(E)** Spatial

spread of second gear episodes. **(F)** Increase of curvature in second gear episodes. Single asterisks denote $P \leq 0.05$, double asterisks denote $P \leq 0.001$ (corrected).

DWELL TIME

The average dwell time of second gear episodes was increased in lesioned animals but not in controls (PD rats: 1.32 ± 0.08 s vs. 1.96 ± 0.35 s, pre- vs. 12 + 28 days postoperatively, $P = 0.01$; control rats: 1.33 ± 0.09 s vs. 1.37 ± 0.15 s, pre- vs. 12 + 28 days postoperatively, $P = 0.84$, corrected; **Figure 5D**). Interestingly, the difference in dwell time was also significant in the 28 days subset of PD rats, but not at 12 days post-surgery ($P = 0.17$ at 12 days vs. $P = 0.01$ at 28 days; $P = 0.05$ for 12 vs. 28 days; corrected). Furthermore, the dwell time of first gear episodes was also significantly prolonged ($P = 0.001$ pre- vs. 12 + 28 days postoperatively, $P = 0.01$ at 12 days, $P = 0.008$ at 28 days; $P = 0.98$ for 12 vs. 28 days; corrected).

SPATIAL SPREAD

The spatial spread accomplished within a given episode (averaged across all second gear episodes of full motion) was increased after 6-OHDA lesioning (PD rats: 17.5 ± 2 cm vs. 22.1 ± 5.3 cm, pre- vs. 12 + 28 days postoperatively, $P = 0.08$; control rats: 18 ± 1.2 cm vs. 18 ± 2.6 cm, pre- vs. postoperatively, $P = 0.83$, corrected; **Figure 5E**). Comparable to the dwell time, the difference was significant at 28 days in PD-rats, but not at 12 days or within the combined group ($P = 1$ at 12 days vs. $P = 0.01$ at 28 days; $P = 0.08$ for 12 vs. 28 days; corrected). Similar to the dwell time, the spatial spread was also significantly enlarged for first gear episodes ($P = 0.001$ pre- vs. 12 + 28 days postoperatively, $P = 0.02$ at 12 days, $P = 0.008$ at 28 days; $P = 0.98$ for 12 vs. 28 days; corrected).

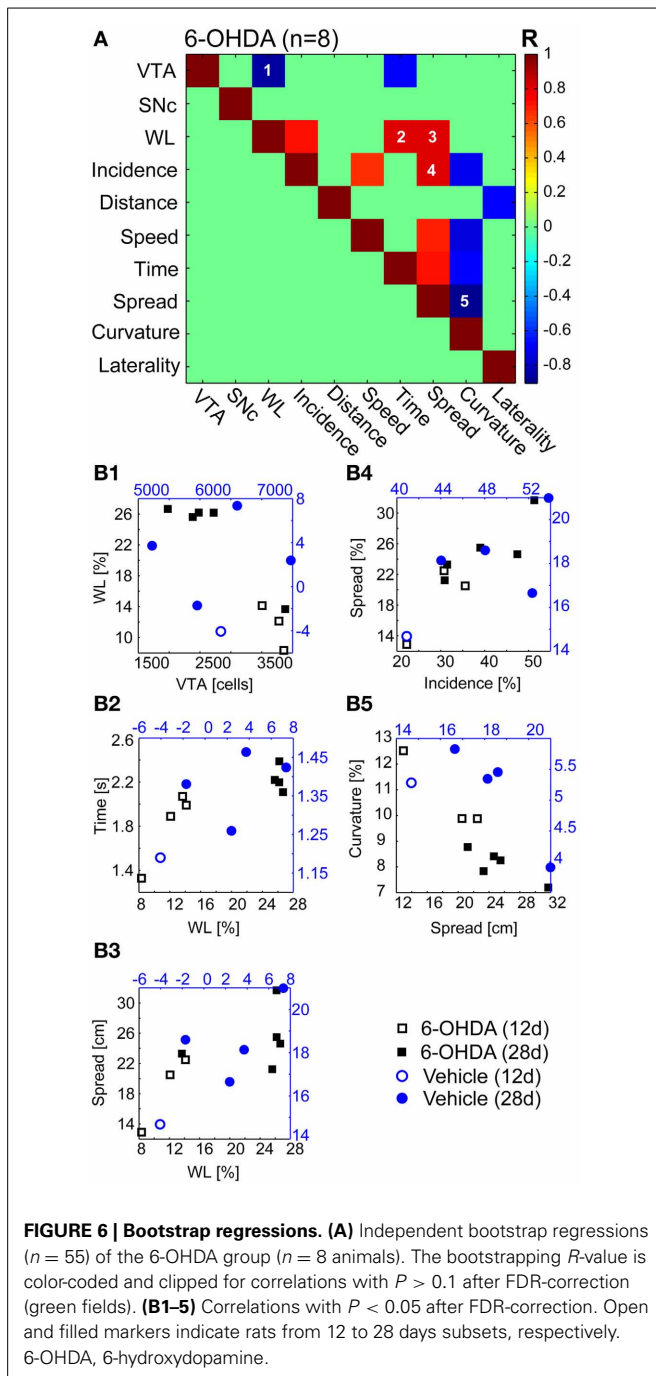
CURVATURE

6-OHDA injections led to an increase of the mean curvature of motion tracks (PD-rats: $4.07 \pm 0.52\%$ vs. $9.15 \pm 1.66\%$, pre- vs.

12 + 28 days postoperatively, $P = 0.002$). Notably, the curvature was also significantly increased in vehicle injected control rats, but only for the comparison of pre vs. combined postoperative groups ($3.850 \pm 0.70\%$ vs. $5.15 \pm 0.64\%$, pre- vs. 12 + 28 days postoperatively, $P = 0.02$, corrected; **Figure 5F**). However, in PD rats we saw a stronger increase 12 days after injections ($P = 0.02$ at 12 days) and a significant recovery of curvature ratios 2 weeks later ($P = 0.05$ for 12 vs. 28 days). At the later time point the ratio was still significantly enhanced ($P = 0.01$ at 28 days). The same pattern of statistically significant differences was observed for first gear episodes ($P = 0.001$ pre- vs. 12 + 28 days postoperatively, $P = 0.01$ at 12 days, $P = 0.008$ at 28 days; $P = 0.05$ for 12 vs. 28 days; corrected).

BOOTSTRAP REGRESSIONS

We found a significant correlation for five of 55 independent comparisons (**Figure 6A**) in 6-OHDA treated rats ($n = 8$). The estimated number of VTA, but not of SNc neurons correlated negatively with the magnitude of weight reduction ($R = -0.86$, **Figure 6B1**). Weight loss also correlated with dwell time ($R = 0.8$, **Figure 6B2**) and spatial spread ($R = 0.8$, **Figure 6B3**). Spatial spread also correlated with the incidence of second gear episodes ($R = 0.71$, **Figure 6B4**). Furthermore, the curvature of motion tracks obtained postoperatively correlated negatively with the spatial spread ($R = -0.9$, **Figure 6B5**). Further 9 comparisons were found statistically significant before FDR-correction and yielded P -values < 0.1 after correction (**Figure 6A**). Among them was the only comparison, incidence of second gear episodes vs. maximal speed, that was also found highly correlated in vehicle injected controls ($R = 1$, data not shown).



DISCUSSION

The main findings of our study are that the stereotypical locomotion pattern of rats exhibiting a first and a second gear of motion is partially lost after bilateral dopaminergic denervation. The reduced incidence of second gear episodes points at distinct deficits in the execution of fast motor sequences. However, although generally slowed, bilaterally lesioned rats also displayed bouts of spontaneous locomotion, to some degree similar to kinesia paradoxa observed in PD patients. Contrary to expectation, we observed an abnormally increased spatial spread and increased

motion time during episodes of full motion in lesioned rats. Moreover, we noted larger curvature values in movement paths of lesioned rats. Upon acceleration, curvature values showed a reduction toward physiological values. All these changes were accompanied by an alteration of circadian locomotor activity.

The depletion of estimated dopaminergic cell populations in the SNc and VTA in our disease model was comparable to that observed in humans suffering from advanced PD, where the VTA is known to be significantly less depleted than the SNc (Hirsch et al., 1988). However, the mesocorticolimbic dopamine projections are vulnerable in advanced PD as well, and seem to contribute to the complex clinical picture encountered in humans, especially at later disease stages (Thobois et al., 2010). It is worth mentioning that our stereological results were similar to cell-loss estimates of 40–50% in the VTA described in human postmortem studies (Uhl et al., 1985; Hirsch et al., 1988; Dymecki et al., 1996; McRitchie et al., 1997; Thobois et al., 2010). The estimated number of SNc neurons of vehicle injected rats in our study was comparable to the number of TH-positive cells reported by a previous study (Fox et al., 2001) that investigated Fisher 344 \times Brown Norway hybrids. Other studies reported significantly higher TH-positive cell counts in different rat strains (Lewis rats, Strackx et al., 2008; Long-Evans rats Healy-Stoffel et al., 2012; Sprague-Dawley rats, Walker et al., 2012) suggesting large differences in the absolute number of midbrain dopaminergic cells in different rat strains.

PD rats in our study displayed a considerable reduction of body weight ($\sim 20\%$). Weight loss and associated metabolic changes might by themselves have an influence on locomotion. We included the reduction of body weight into multiple bootstrap regressions and investigated the interdependence between behavioral endpoints, dopaminergic cell loss and weight reduction. We found a significant negative correlation between the VTA, but not the SNc dopaminergic population, and the magnitude of weight loss. Thus, abnormal feeding behavior and more generally abulia, was related to cell loss within the mesolimbic dopaminergic system in our study (Redgrave et al., 2010).

Our analysis approach allowed the discrimination of naturally occurring motion episodes in severely dopamine depleted and overtly akinetic and bradykinetic rats. The characterization of motion episodes by the maximal rather than the average speed accomplished in a given episode enabled us to analyze rare and, given the pronounced parkinsonian phenotype of our rats, unexpected episodes of qualitatively altered motor activity. These motion episodes were still characterized by a reduced incidence (i.e., poverty of movement or akinesia), reduced overall traveled distance (i.e., hypokinesia) and reduced maximal speed (i.e., bradykinesia) compared to controls. Hence, important hallmark symptoms of PD were clearly detectable in motion episodes of 6-OHDA rats. However, we did not see a significant correlation of these three behavioral endpoints with the estimated populations of the SNc and VTA.

Overall, the quantitative change in traveled distance was rather small. A disruption of the circadian rhythm, a cardinal non-motor symptom in human PD patients (Videnovic and Golombek, 2013) and present in animal models of PD (Kudo et al., 2011; Willison et al., 2013) may introduce a bias. Higher

absolute activity values may result from prolongation and fragmentation of activity and reduced sleep phases. Our analysis method could not differentiate between awake resting and true sleep, but conclusions could still be drawn from the overall circadian activity pattern. Here, we observed a more fragmented pattern of activity together with a nearly absent second activity phase. Moreover, PD rats showed a significantly reduced absolute number of motion episodes in comparison to controls (data not shown). Together, this argues against a circadian bias toward higher distance values in our data.

The finding of increased dwell times and spatial spread in first and second gear motion episodes of PD rats was rather unexpected. The spatial spread in the 6-OHDA group was increased to values not seen in any pre-lesion or control recordings. Theoretically, an increased dwell time could be explained as a function of slowed locomotion. To reach the same location, bradykinetic rats may simply need more time. This interdependence should theoretically manifest in a negative correlation between speed and dwell time or spatial spread. To the contrary, our data revealed a positive correlation between speed and spatial spread, albeit not significant after FDR-correction. That is, faster PD rats showed spatially extended second gear episodes. Could a postlesion increase in curvature explain increased dwell times? Arguing against that, curvature values were significantly negatively correlated with spatial spread, and also with dwell time, speed and incidence of second gear episodes (before FDR-correction). Furthermore, a higher incidence of second gear behavior correlated significantly with prolonged spatial spread. Such an increased incidence could be the result of an uneven effect of 6-OHDA lesioning and stronger diminishment of first gear in comparison to second gear activity. This would also be supported by the finding that 6-OHDA induced weight loss correlated positively with the incidence of second gear activity (before FDR-correction). Taken together, increased spatial spread and dwell times constitute an abnormal behavioral characteristic of PD rats.

An abnormal increase of locomotor activity in bilaterally lesioned rats has been described in response to a pharmacological challenge (Schallert et al., 1978). Unexpected bursts of locomotion in otherwise akinetic patients are also well known to occur in selected PD patients or cases with postencephalitic parkinsonism (kinesia paradoxa). The sudden ability of our rats to cover longer distances within a motion episode may thus represent a rat equivalent of this condition. There are, however, important differences to classical kinesia paradoxa, which is often triggered by external sensory cues (Martin, 1967).

One possible explanation for prolonged dwell times and increased spatial spread could be problems with the termination of movement. In PD patients, deficiency in smooth motion termination is known (Dounskaia et al., 2009), along with an inability to promptly change generated force or quickly re-plan current motion. Typically, PD patients show an asymmetric evolution of velocities during the execution of goal-directed behaviors with initial fast accelerations (Flash et al., 1992). In our data we found a symmetric evolution of acceleration between PD and control rats. That is, we saw a linear relationship between the dwell time and the time point where PD or control rats accomplished their

maximal speed in a given episode (data not shown). Thus, the observed behavioral abnormalities do not support the presence of the hastening phenomenon (unwanted acceleration of movement in human PD patients) in our rats. Finally, it is also conceivable that the abnormal drive to continue exploration or food search could be a behavioral consequence of metabolic changes accompanying weight loss (Redgrave et al., 2010).

Another abnormal feature was found in the movement path's curvature. The ratio between real and direct distance of first and second gear motion episodes was significantly enlarged in PD rats and, to a lesser extent, in controls. What could be the cause of increased curvatures? Unilaterally depleted rats display a spontaneous ipsiversive motor bias (Ungerstedt, 1971). Hence, curvature increases could result from spontaneous partial turning behavior provoked by asymmetric dopaminergic lesioning in our rats. However, the calculated LI did not correlate with curvature or any other behavioral endpoint except distance (before FDR-correction). Furthermore, unilateral 6-OHDA lesions were shown to shorten steps in spontaneous walking (Metz et al., 2005), thus modeling the shuffling gait of PD patients (Knutsson, 1972). Hind limb rigidity was detected upon manual assessment in our PD rats and could have contributed to disturbed locomotor patterns with reduced step sizes, axial instability and loss of balance during walking. Hemiparkinsonian rats, when tested by e.g., beam-walking, also exhibit difficulties in motor coordination (Truong et al., 2006). Interestingly, we found a significant negative correlation between curvature and spatial spread, as well as maximal speed, dwell time and incidence of second gear activity (before FDR-correction). Thus, faster running or greater spreads were associated with straighter movement paths in PD rats. If limb rigidity was indeed related to the expression of increased curvature values, then the ability of PD rats to generate fast motion with reduced curvature values may reflect an overcoming of rigidity for brief periods.

We saw some differences between lesioned animals that were monitored at an early (12 days) and later stage (28 days) after 6-OHDA lesioning. Most strikingly, the dwell time was significantly longer at 28 days in comparison with 12 days postlesion. Contrary, curvature increases significantly decreased again at the later point of investigation. Importantly, no significant difference in cell counts was observed between the two subsets. It remains difficult to infer which compensatory mechanisms were at work here. The milder but still significant increase of curvature in controls, in conjunction with the significant decrease of curvature values in PD rats with time, could argue for an influence of and recovery from surgery *per se*. The emergence of an abnormally increased behavior such as kinesia paradoxa may have in turn developed over time when the rats recovered fully from surgery. Despite putative effects of recovery from surgery, absolute distance, speed and incidence of second gear activity were comparably decreased at an early and later point of investigation.

We conclude that long-term behavioral observations of spontaneous locomotion offers new perspectives on distinctly different modes of motion in a rat model of advanced PD. The present behavioral analysis, in conjunction with *in-vivo* electrophysiology, may be particularly suited to reveal neural mechanisms underlying motor fluctuations such as kinesia

paradoxa, and may provide further insights into the complex pathophysiology of PD.

AUTHOR CONTRIBUTIONS

Benjamin Grieb, Gerhard Engler, Ismini Papageorgiou, Wolfgang Hamel, and Christian K. Moll designed research; Benjamin Grieb, Gerhard Engler, and Ismini Papageorgiou performed experiments; Benjamin Grieb, Constantin von Nicolai, Andrew Sharott, and Ismini Papageorgiou analyzed the data; Benjamin Grieb, Constantin von Nicolai, Andrew Sharott, Andreas K. Engel, and Christian K. Moll wrote the manuscript.

ACKNOWLEDGMENTS

The authors would like to thank Doris Lange for help with the histology. This work was supported by the European Union (MRTN-CT-2005-019247).

REFERENCES

- Avila, I., Parr-Brownlie, L. C., Brazhnik, E., Castañeda, E., Bergstrom, D. A., and Walters, J. R. (2010). Beta frequency synchronization in basal ganglia output during rest and walk in a hemiparkinsonian rat. *Exp. Neurol.* 221, 307–319. doi: 10.1016/j.expneurol.2009.11.016
- Belujon, P., Bezard, E., Taupignon, A., Bioulac, B., and Benazzouz, A. (2007). Noradrenergic modulation of subthalamic nucleus activity: behavioral and electrophysiological evidence in intact and 6-hydroxydopamine-lesioned rats. *J. Neurosci.* 27, 9595–9606. doi: 10.1523/JNEUROSCI.2583-07.2007
- Benjamini, Y., and Hochberg, Y. (1995). Controlling the false discovery rate: a practical and powerful approach to multiple testing. *J. R. Stat. Soc. B* 57, 289–300. doi: 10.2307/2346101
- Bergman, H., Wichmann, T., and DeLong, M. R. (1990). Reversal of experimental parkinsonism by lesions of the subthalamic nucleus. *Science* 249, 1436–1438. doi: 10.1126/science.2402638
- Brazhnik, E., Cruz, A. V., Avila, I., Wahba, M. I., Novikov, N., Ilieva, N. M., et al. (2012). State-dependent spike and local field synchronization between motor cortex and substantia nigra in hemiparkinsonian rats. *J. Neurosci.* 32, 7869–7880. doi: 10.1523/JNEUROSCI.0943-12.2012
- Cass, W. A., Peters, L. E., and Smith, M. P. (2005). Reductions in spontaneous locomotor activity in aged male, but not female, rats in a model of early Parkinson's disease. *Brain Res.* 1034, 153–161. doi: 10.1016/j.brainres.2004.12.009
- Cenci, M. A., Whishaw, I. Q., and Schallert, T. (2002). Animal models of neurological deficits: how relevant is the rat? *Nat. Rev. Neurosci.* 3, 574–579. doi: 10.1038/nrn877
- Dounskaia, N., Fradet, L., Lee, G., Leis, B. C., and Adler, C. H. (2009). Submovements during pointing movements in Parkinson's disease. *Exp. Brain Res.* 193, 529–544. doi: 10.1007/s00221-008-1656-6
- Drai, D., Benjamini, Y., and Golani, I. (2000). Statistical discrimination of natural modes of motion in rat exploratory behavior. *J. Neurosci. Methods* 96, 119–131. doi: 10.1016/S0165-0270(99)00194-6
- Drai, D., and Golani, I. (2001). SEE: a tool for the visualization and analysis of rodent exploratory behavior. *Neurosci. Biobehav. Rev.* 25, 409–426. doi: 10.1016/S0149-7634(01)00022-7
- Drai, D., Kafkafi, N., Benjamini, Y., Elmer, G., and Golani, I. (2001). Rats and mice share common ethologically relevant parameters of exploratory behavior. *Behav. Brain Res.* 125, 133–140. doi: 10.1016/S0166-4328(01)00290-X
- Dymecki, J., Lechowicz, W., Bertrand, E., and Szpak, G. M. (1996). Changes in dopaminergic neurons of the mesocorticolimbic system in Parkinson's disease. *Folia Neuropathol.* 34, 102–106.
- Ferro, M. M., Bellissimo, M. I., Anselmo-Franci, J. A., Angellucci, M. E., Canteras, N. S., and Da Cunha, C. (2005). Comparison of bilaterally 6-OHDA- and MPTP-lesioned rats as models of the early phase of Parkinson's disease: histological, neurochemical, motor and memory alterations. *J. Neurosci. Methods* 148, 78–87. doi: 10.1016/j.jneumeth.2005.04.005
- Flash, T., Inzelberg, R., Schechtman, E., and Korczyn, A. D. (1992). Kinematic analysis of upper limb trajectories in Parkinson's disease. *Exp. Neurol.* 118, 215–226. doi: 10.1016/0014-4886(92)90038-R
- Fox, C. M., Gash, D. M., Smoot, M. K., and Cass, W. A. (2001). Neuroprotective effects of GDNF against 6-OHDA in young and aged rats. *Brain Res.* 896, 56–63. doi: 10.1016/S0006-8993(00)03270-4
- Gundersen, H. J. (1986). Stereology of arbitrary particles. a review of unbiased number and size estimators and the presentation of some new ones, in memory of William R. Thompson. *J. Microsc.* 143(Pt 1), 3–45. doi: 10.1111/j.1365-2818.1986.tb02764.x
- Gundersen, H. J., and Jensen, E. B. (1987). The efficiency of systematic sampling in stereology and its prediction. *J. Microsc.* 147(Pt 3), 229–263. doi: 10.1111/j.1365-2818.1987.tb02837.x
- Healy-Stoffel, M., Ahmad, S. O., Stanford, J. A., and Levant, B. (2012). A novel use of combined tyrosine hydroxylase and silver nucleolar staining to determine the effects of a unilateral intrastriatal 6-hydroxydopamine lesion in the substantia nigra: a stereological study. *J. Neurosci. Methods* 210, 187–194. doi: 10.1016/j.jneumeth.2012.07.013
- Hirsch, E., Graybiel, A. M., and Agid, Y. A. (1988). Melanized dopaminergic neurons are differentially susceptible to degeneration in Parkinson's disease. *Nature* 334, 345–348. doi: 10.1038/334345a0
- Kelly, P. H. (1975). Unilateral 6-hydroxydopamine lesions of nigrostriatal or mesolimbic dopamine-containing terminals and the drug-induced rotation of rats. *Brain Res.* 100, 163–169. doi: 10.1016/0006-8993(75)90253-X
- Knutsson, E. (1972). An analysis of Parkinsonian gait. *Brain* 95, 475–486. doi: 10.1093/brain/95.3.475
- Kudo, T., Loh, D. H., Truong, D., Wu, Y., and Colwell, C. S. (2011). Circadian dysfunction in a mouse model of Parkinson's disease. *Exp. Neurol.* 232, 66–75. doi: 10.1016/j.expneurol.2011.08.003
- Martin, J. P. (1967). *The Basal Ganglia and Posture*. Philadelphia, PA: Lippincott.
- McRitchie, D. A., Cartwright, H. R., and Halliday, G. M. (1997). Specific A10 dopaminergic nuclei in the midbrain degenerate in Parkinson's disease. *Exp. Neurol.* 144, 202–213. doi: 10.1006/exnr.1997.6418
- Metz, G. A., Tse, A., Ballermann, M., Smith, L. K., and Fouad, K. (2005). The unilateral 6-OHDA rat model of Parkinson's disease revisited: an electromyographic and behavioural analysis. *Eur. J. Neurosci.* 22, 735–744. doi: 10.1111/j.1460-9568.2005.04238.x
- Mokry, J. (1995). Experimental models and behavioural tests used in the study of Parkinson's disease. *Physiol. Res.* 44, 143–150.
- Paxinos, G., and Watson, C. (2005). *The Rat Brain in Stereotaxic Coordinates*. 5th Edn. Sydney, NSW: Academic Press.
- Redgrave, P., Rodriguez, M., Smith, Y., Rodriguez-Oroz, M. C., Lehericy, S., Bergman, H., et al. (2010). Goal-directed and habitual control in the basal ganglia: implications for Parkinson's disease. *Nat. Rev. Neurosci.* 11, 760–772. doi: 10.1038/nrn2915
- Sakai, K., and Gash, D. M. (1994). Effect of bilateral 6-OHDA lesions of the substantia nigra on locomotor activity in the rat. *Brain Res.* 633, 144–50. doi: 10.1016/0006-8993(94)91533-4
- Schallert, T., Whishaw, I. Q., Ramirez, V. D., and Teitelbaum, P. (1978). Compulsive, abnormal walking caused by anticholinergics in akinetic, 6-hydroxydopamine-treated rats. *Science* 199, 1461–1463. doi: 10.1126/science.564552
- Schwartz, R. K., and Huston, J. P. (1996a). Unilateral 6-hydroxydopamine lesions of meso-striatal dopamine neurons and their physiological sequelae. *Prog. Neurobiol.* 49, 215–266. doi: 10.1016/S0301-0082(96)00015-9
- Schwartz, R. K., and Huston, J. P. (1996b). The Unilateral 6-hydroxydopamine lesion model in behavioral brain research. Analysis of functional deficits, recovery and treatments. *Prog. Neurobiol.* 50, 275–331. doi: 10.1016/S0301-0082(96)00040-8
- Seghier, M. L. (2008). Laterality index in functional MRI: methodological issues. *Magn. Reson. Imaging* 26, 594–601. doi: 10.1016/j.mri.2007.10.010
- Strackx, E., Van den Hove, D. L., Steinbusch, H. P., Steinbusch, H. W., Vles, J. S., Blanco, C. E., et al. (2008). A combined behavioral and morphological study on the effects of fetal asphyxia on the nigrostriatal dopaminergic system in adult rats. *Exp. Neurol.* 211, 413–422. doi: 10.1016/j.expneurol.2008.02.006
- Thobois, S., Ardouin, C., Lhommée, E., Klingler, H., Lagrange, C., Xie, J., et al. (2010). Non-motor dopamine withdrawal syndrome after surgery for Parkinson's disease: predictors and underlying mesolimbic denervation. *Brain* 133(Pt. 4), 1111–1127. doi: 10.1093/brain/awq032
- Truong, L., Allbutt, H., Kassiou, M., and Henderson, J. M. (2006). Developing a preclinical model of Parkinson's disease: a study of behaviour in rats with graded 6-OHDA lesions. *Behav. Brain Res.* 169, 1–9. doi: 10.1016/j.bbr.2005.11.026

- Uhl, G. R., Hedreen, J. C., and Price, D. L. (1985). Parkinson's disease: loss of neurons from the ventral tegmental area contralateral to therapeutic surgical lesions. *Neurology* 35, 1215–1218.
- Ungerstedt, U. (1971). Postsynaptic supersensitivity after 6-hydroxy-dopamine induced degeneration of the nigro-striatal dopamine system. *Acta Physiol. Scand. Suppl.* 367, 69–93.
- Videnovic, A., and Golombek, D. (2013). Circadian and sleep disorders in Parkinson's disease. *Exp. Neurol.* 243, 45–56. doi: 10.1016/j.expneurol.2012.08.018
- Walker, Q. D., Johnson, M. L., Van Swearingen, A. E., Arrant, A. E., Caster, J. M., and Kuhn, C. M. (2012). Individual differences in psychostimulant responses of female rats are associated with ovarian hormones and dopamine neuroanatomy. *Neuropharmacology* 62, 2267–2277. doi: 10.1016/j.neuropharm.2012.01.029
- West, M. J. (2002). Design-based stereological methods for counting neurons. *Prog. Brain Res.* 135, 43–51. doi: 10.1016/S0079-6123(02)35006-4
- West, M. J., Slomianka, L., and Gundersen, H. J. (1991). Unbiased stereological estimation of the total number of neurons in the subdivisions of the rat hippocampus using the optical fractionator. *Anat. Rec.* 231, 482–497. doi: 10.1002/ar.1092310411
- Willison, L. D., Kudo, T., Loh, D. H., Kuljis, D., and Colwell, C. S. (2013). Circadian dysfunction may be a key component of the non-motor symptoms of Parkinson's disease: insights from a transgenic mouse model. *Exp. Neurol.* 243, 57–66. doi: 10.1016/j.expneurol.2013.01.014
- Conflict of Interest Statement:** The authors declare that the research was conducted in the absence of any commercial or financial relationships that could be construed as a potential conflict of interest.
- Received: 01 September 2013; accepted: 08 November 2013; published online: 27 November 2013.
- Citation: Grieb B, von Nicolai C, Engler G, Sharott A, Papageorgiou I, Hamel W, Engel AK and Moll CK (2013) Decomposition of abnormal free locomotor behavior in a rat model of Parkinson's disease. *Front. Syst. Neurosci.* 7:95. doi: 10.3389/fnsys.2013.00095
- This article was submitted to the journal *Frontiers in Systems Neuroscience*. Copyright © 2013 Grieb, von Nicolai, Engler, Sharott, Papageorgiou, Hamel, Engel and Moll. This is an open-access article distributed under the terms of the Creative Commons Attribution License (CC BY). The use, distribution or reproduction in other forums is permitted, provided the original author(s) or licensor are credited and that the original publication in this journal is cited, in accordance with accepted academic practice. No use, distribution or reproduction is permitted which does not comply with these terms.

Part B

**High-frequency stimulation of the subthalamic nucleus counteracts
cortical expression of major histocompatibility complex genes
in a rat model of Parkinson's disease**

Published in PLoS ONE on March 12, 2014

High-Frequency Stimulation of the Subthalamic Nucleus Counteracts Cortical Expression of Major Histocompatibility Complex Genes in a Rat Model of Parkinson's Disease

Benjamin Grieb^{1,5*}, Gerhard Engler¹, Andrew Sharott¹, Constantin von Nicolai^{1,6}, Thomas Streichert², Ismini Papageorgiou³, Alexander Schulte⁴, Manfred Westphal⁴, Katrin Lamszus⁴, Andreas K. Engel¹, Christian K. E. Moll^{1,9}, Wolfgang Hamel^{4,9}

1 Department of Neurophysiology and Pathophysiology, University Medical Center Hamburg-Eppendorf, Hamburg, Germany, **2** Department of Clinical Chemistry, University Medical Center Hamburg-Eppendorf, Hamburg, Germany, **3** Division of General Neurophysiology, Institute of Physiology and Pathophysiology, University of Heidelberg, Heidelberg, Germany, **4** Department of Neurosurgery, University Medical Center Hamburg-Eppendorf, Hamburg, Germany, **5** Department of General Psychiatry, Center for Psychosocial Medicine, University of Heidelberg, Heidelberg, Germany, **6** Centre for Integrative Neuroscience, University of Tübingen, Tübingen, Germany

Abstract

High-frequency stimulation of the subthalamic nucleus (STN-HFS) is widely used as therapeutic intervention in patients suffering from advanced Parkinson's disease. STN-HFS exerts a powerful modulatory effect on cortical motor control by orthodromic modulation of basal ganglia outflow and via antidromic activation of corticofugal fibers. However, STN-HFS-induced changes of the sensorimotor cortex are hitherto unexplored. To address this question at a genomic level, we performed mRNA expression analyses using Affymetrix microarray gene chips and real-time RT-PCR in sensorimotor cortex of parkinsonian and control rats following STN-HFS. Experimental parkinsonism was induced in Brown Norway rats by bilateral nigral injections of 6-hydroxydopamine and was assessed histologically, behaviorally, and electrophysiologically. We applied prolonged (23h) unilateral STN-HFS in awake and freely moving animals, with the non-stimulated hemisphere serving as an internal control for gene expression analyses. Gene enrichment analysis revealed strongest regulation in major histocompatibility complex (MHC) related genes. STN-HFS led to a cortical downregulation of several MHC class II (RT1-Da, Db1, Ba, and Cd74) and MHC class I (RT1CE) encoding genes. The same set of genes showed increased expression levels in a comparison addressing the effect of 6-hydroxydopamine lesioning. Hence, our data suggest the possible association of altered microglial activity and synaptic transmission by STN-HFS within the sensorimotor cortex of 6-hydroxydopamine treated rats.

Citation: Grieb B, Engler G, Sharott A, von Nicolai C, Streichert T, et al. (2014) High-Frequency Stimulation of the Subthalamic Nucleus Counteracts Cortical Expression of Major Histocompatibility Complex Genes in a Rat Model of Parkinson's Disease. *PLoS ONE* 9(3): e91663. doi:10.1371/journal.pone.0091663

Editor: Lucio Annunziato, University of Naples Federico II, Italy

Received: November 10, 2012; **Accepted:** February 14, 2014; **Published:** March 12, 2014

Copyright: © 2014 Grieb et al. This is an open-access article distributed under the terms of the Creative Commons Attribution License, which permits unrestricted use, distribution, and reproduction in any medium, provided the original author and source are credited.

Funding: The study received intramural funding from the University Medical Center Hamburg-Eppendorf. The funders had no role in study design, data collection and analysis, decision to publish, or preparation of the manuscript.

Competing Interests: The authors have declared that no competing interests exist.

* E-mail: benjamin.grieb@med.uni-heidelberg.de

⁹ These authors contributed equally to this work.

Introduction

In Parkinson's disease (PD), nigrostriatal dopamine depletion is the source of severe disturbances within skeletomotor loops that tightly link cortex, basal ganglia and thalamus [1,2]. Pathological activity originating anywhere in these loops disrupts physiological processing at the level of the sensorimotor cortex and aberrant or missing corticofugal motor commands lead to the emergence of cardinal motor signs in PD, such as akinesia, rigidity and resting tremor. During the last two decades, chronic high-frequency stimulation (HFS, also termed deep brain stimulation, DBS) of the subthalamic nucleus (STN) has emerged as a safe and effective treatment option for medically refractory PD patients [3,4]. Although the efficacy of STN-HFS in treating PD has been conclusively shown, there are significant differences in the latencies

for the amelioration of the abovementioned motor symptoms. While an improvement of rigidity typically occurs immediately and remains stable throughout continuous STN-HFS over several months, an amelioration of resting tremor, bradykinesia and off-drug dystonia is often observed with different latencies ranging from seconds to weeks of continuous HFS [5]. Moreover, return to baseline symptom severity is variable after HFS-offset [6]. Such latency differences and carry-over effects suggest that in addition to immediate electrophysiological or neurochemical modulation of neuronal activity, HFS leads to adaptive and plastic changes on a longer time-scale. This view is supported by experimental evidence that STN-HFS induces synaptic plasticity in the rat STN [7] and mediates neuroprotection on substantia nigra dopaminergic neurons in a model of neurotoxin-induced degeneration [8,9].

In order to understand the mechanism of action of STN-HFS, a multitude of studies have focused on its immediate consequences on neural activity in different interconnected structures. While some studies favor an involvement of cortico-basal ganglia loops [10,11], a different view highlights the importance of a retrograde cortical activation via the “hyperdirect” pathway containing projections from frontal cortical areas to the STN [12–14]. In fact, a recent study demonstrated that sensorimotor cortex is antidromically activated by STN-HFS [15]. This activation may be of critical importance for amelioration of motor deficits induced by nigrostriatal dopamine depletion [16,17]. Consistent with this, scalp potentials with short latency have been recorded from surgically treated patients during both low [18–21] and high frequency STN stimulation [22].

Whatever the mechanism, virtually all hypotheses converge upon a close involvement of the cerebral cortex in the mediation of STN-HFS effects, as the motor cortex is the origin of the final common pathway for all motor symptoms. While it is clear that STN-HFS immediately alters the discharge characteristics in remote brain areas such as sensorimotor cortex, the long-term adaptive impact of such changes is not clear, and studies investigating the impact of therapeutic STN-HFS on remote brain areas at the molecular level are sparse. We have previously shown that STN-HFS increases the expression of immediate early genes in various nuclei of the basal ganglia and the sensorimotor cortex of naïve rats [23], indicating enhanced neuronal activity in these areas [24]. A recent genetic screening study applied chronic HFS to the thalamus of naïve rats with a focus on changes in hippocampus, striatum and motor cortex [25]. Another study investigated the effects of STN-HFS on gene expression within the basal ganglia of anesthetized hemiparkinsonian rats [26]. However, STN-HFS-associated gene expression changes at the cortical level of awake, parkinsonian animals are hitherto unexplored. Therefore, the present study was specifically designed to elaborate the impact of STN-HFS on sensorimotor cortex at the molecular level in a bilateral PD rat model.

To this end, we employed prolonged unilateral STN-HFS (23 h) in awake and unrestrained rats rendered parkinsonian by means of bilateral 6-hydroxydopamine (6-OHDA) injections into the substantia nigra pars compacta (SNc). Our animal model was characterized in detail by a multi-modal approach consisting of histology, behavioral analysis of locomotion and both intraoperative and postoperative electrophysiology. Affymetrix microarrays and real time RT-PCR analysis were utilized to identify genes regulated by STN-HFS in tissue samples taken from the rat sensorimotor cortex. Western blotting was utilized to investigate protein levels of selected candidate genes.

Materials and Methods

Animal model and experimental design

Experiments were approved by the local government authorities of Hamburg (Germany; Behörde für Soziales, Familie, Gesundheit und Verbraucherschutz; Fachabteilung für Lebensmittelsicherheit und Veterinärwesen) and carried out in accordance with the European Council Directive 86/609/EEC. All surgeries were performed under ketamine/xylazine anesthesia and all efforts were made to minimize suffering. We randomly assigned 20 male Brown Norway rats (*Rattus norvegicus*; Charles River Laboratories, Sulzfeld, Germany) to two different experimental groups (see Figure 1): A PD group with 12 rats receiving bilateral 6-OHDA injections into the SNc for induction of experimental parkinsonism [27,28] and a control group with eight rats receiving bilateral vehicle injections. High mortality rates due to abulia and weight

loss are known from bilateral 6-OHDA rats [29]. Therefore, all rats were monitored on a daily basis and offered a soft and moist rat chow and 10%-glucose solution in addition to standard chow and water ad libitum. To sustain aphagic and adipsic PD rats in the most critical post-operative phase, we administered a liquid and high caloric nutrition for rodents (Altromin, Lage, Germany) by manual needle feeding. Animals received s.c.-injections of metamizole (100 mg/kg, Medistar, Holzwickede, Germany) for postoperative analgesia following surgery and on behavioral signs of pain distress (e.g., vocalization upon gentle palpation or self-mutilation such as licking, biting, scratching or other form of harming body parts). Daily inspections took place until three weeks after each surgery. Spontaneous locomotor activity was assessed prior to and three weeks after 6-OHDA lesions. In a second surgery eleven weeks after 6-OHDA injections, we implanted 15 rats ($n=7$ PD and $n=8$ controls) with bilateral stimulation electrodes into both STNs. Recordings of cortical and subthalamic local field potentials (LFP) took place 12–13 weeks after 6-OHDA lesions. Gene expression profiling following 23 hours of STN-HFS was subsequently carried out 14 weeks after 6-OHDA lesions in a subset of six animals ($n=3$ PD, $n=3$ controls). Drop outs included perioperative death ($n=2$ controls), loss of implant ($n=3$ PD) and euthanasia by cervical dislocation under deep anesthesia (i.p.-injection of ketamine 100 mg/kg, xylazine 6 mg/kg) following loss of >20% body weight without stabilization of weight loss within 14 days after surgery ($n=3$ PD), development of severe dystonia ($n=1$ PD), neoplasia ($n=1$ control) or broken stimulation leads ($n=1$ PD, $n=1$ control).

Bilateral 6-hydroxydopamine lesions

Stereotactic surgery was performed in rats (preoperative weight: 384 ± 32 g, mean \pm SD) under general anesthesia. 30 minutes prior to 6-OHDA or vehicle injections, rats received a bolus i.p.-injection of desipramine (25 mg/kg, Sigma-Aldrich, Munich, Germany) to minimize uptake of 6-OHDA in noradrenergic midbrain neurons [27]. Anesthesia was introduced with isoflurane (Baxter Germany GmbH, Unterschleißheim, Germany) and maintained with i.p.-injections of ketamine (65 mg/kg, Dr. E. Gräub AG, Bern, Switzerland) and xylazine (3 mg/kg, Bayer

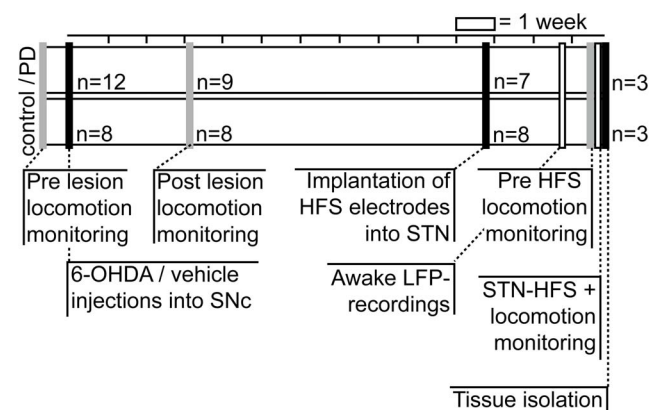


Figure 1. Flowchart of the experimental design. The sequence of experimental steps (i.e., 6-OHDA or vehicle injections, pre- and post-operative locomotion monitoring, STN-HFS electrode implantation, awake LFP recordings, pre-HFS locomotion monitoring, awake STN-HFS under locomotion monitoring, tissue isolation), number of included animals and time between steps is given in a flowchart. 6-OHDA, 6-hydroxydopamine; STN, subthalamic nucleus, HFS, high-frequency stimulation; LFP, local field potential.

doi:10.1371/journal.pone.0091663.g001

Health Care, Leverkusen, Germany). An initial bolus of atropine (0.25 mg/kg, B. Braun Melsungen AG, Melsungen, Germany) was administered for cardiopulmonary protection. During surgery we monitored body temperature with a rectal probe and prevented hypothermia with an adjustable heating pad (FST, Heidelberg, Germany). In addition, the eyes were covered with dexpanthenol cream to prevent exsiccation. Animals were mounted in a stereotactic frame (David Kopf Instruments, Tujunga, USA) to target the SNc at +4 mm AP and ± 2.2 mm ML using the interaural line as reference [30]. After placement of burr holes, a Hamilton microliter-syringe (FST) was lowered to the target depth at -8 mm relative to the dura. $5 \mu\text{l}$ neurotoxin ($3 \mu\text{g}/\mu\text{l}$ 6-OHDA in 0.2% ascorbic acid solution, stored on ice; Sigma-Aldrich) or vehicle (aqua injectabilia, 0.2% ascorbic acid solution; Sigma-Aldrich) was slowly infused at a rate of $0.5 \mu\text{l}/\text{min}$ and the syringe was left in place for two minutes to allow for complete absorption of the toxin. The burr hole was closed with bone wax and the procedure was repeated in the contralateral hemisphere.

Implantation of STN electrodes

STN electrodes were implanted in a second surgery 54 ± 11 days after SNc surgery in 15 rats ($n = 7$ PD; $n = 8$ controls; see Figure 1). The experimental design incorporated a long time window between the first and second surgery to allow PD rats to fully recover from lesioning. Fine needle electromyography electrodes (Technomed, Beek, The Netherlands) were customized for prolonged application of STN-HFS [31]. To minimize risk of electrical tissue damage during HFS, electrodes consisted of a gold-plated stainless steel cannula ($350 \mu\text{m}$ shaft diameter, isolated with coating varnish, Beck Electrical Insulation, Hamburg, Germany) with an isolated inlay of platinum-iridium wire ($50 \mu\text{m}$ tip diameter, cathode). Furthermore, each electrode tip was checked microscopically to ensure that the platinum-iridium inlay was completely embedded inside the cannula forming a clean cut surface without sharp edges, thereby avoiding the occurrence of high current densities at the cathode [32]. After exposure of the skull, we drilled two burr holes (1.8 mm diameter; $+5$ mm AP, ± 2.2 mm ML relative to the interaural line) for microelectrode navigation using two tungsten microelectrodes (FHC, Bowdoin, USA; $200\text{--}800$ k Ω impedance; 0.5 mm spacing) mounted on a manual electrode microdrive (Alpha Omega, Nazareth, Israel). Signals from each electrode were pre-amplified, amplified and bandpass filtered ($500\text{--}5000$ Hz, multi-channel processor, Alpha Omega) to extract multi-unit activity. Data were visualized and evaluated online using Spike2 software (Cambridge Electronic Design, Cambridge, UK) to locate the best possible site of electrode placement directly within the STN (see Figure 2A). The STN was identified by the appearance of elevated background activity together with irregular high-frequency firing interspersed with bursting discharges that were clearly different from the low threshold spike bursts encountered en route in the thalamus. A sharp decline of background neuronal activity together with the absence of spike discharges marked the ventral STN border and the transition to subjacent capsular fibers. Planning coordinates ($+5$ mm AP, ± 2.2 mm ML relative to the interaural line and -8 mm DV relative to dura) were adjusted to match the results of microelectrode-guided delineation of STN boundaries. HFS-electrodes were then inserted with a manual microdrive and fixed onto the skull with dental cement (Heraeus Kulzer; Wehrheim, Germany). Four stainless steel screws (FST, 0.7 mm diameter) were anchored around the trepanations to assure long-term stability of the implant. Two stainless steel recording screws (FST, 1 mm diameter) were placed over the frontal cortex ($+11.5$ mm AP, ± 2 mm ML) for chronic recordings of the electrocorticogram

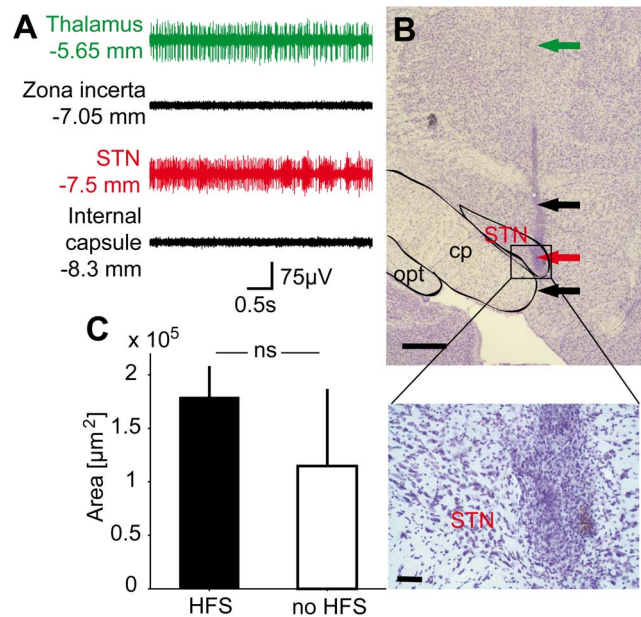


Figure 2. Electrode placement and tissue reaction. Representative traces (A) of microelectrode guided targeting of the STN under ketamine/xylozine anesthesia. Note that the STN trace is characterized by elevated background activity, bursts and irregular high-frequency firing. A representative electrode trajectory (B) targeting the STN (cresyl-violet staining, arrowheads indicate trajectory, scale bar $500 \mu\text{m}$). The STN, cerebral peduncle (cp) and optic tract (opt) are circumscribed with black surrounding lines. Photomicrographs of the STN at 20x- and 40x-magnification (scale bars $100 \mu\text{m}$ and $50 \mu\text{m}$, respectively) reveal mild reactive tissue infiltration with mononuclear cells at the electrode tip. Bars (C) indicate the area (mean \pm SD) infiltrated by mononuclear cells at the tip of stimulated (HFS, black bar) and non-stimulated electrodes (no HFS, white bar; $n = 6$ in each group). STN, subthalamic nucleus; HFS, high-frequency stimulation; cp, cerebral peduncle; opt, optic tract. doi:10.1371/journal.pone.0091663.g002

(ECoG). In addition, two reference screws were anchored centrally over the cerebellum (-3 mm AP, 0 mm ML) and over an area of thickened nasal bone ($+14$ mm AP, 0 mm ML).

Behavioral Monitoring

To assess the efficacy of 6-OHDA lesions in particular with respect to hypo- and bradykinesia and the influence of prolonged unilateral STN-HFS in parkinsonian and control rats we investigated general locomotor capacities via continuous (23h) monitoring of spontaneous behavior. Time points of behavioral recordings were five days prior and 22 ± 8 days after SNc surgery, as well as directly before and during STN-HFS 18 ± 5 days after electrode implantation (see Figure 1). As described previously [33], we used a video-based tracking system (VideoMot 2.0, TSE Systems, Bad Homburg, Germany) to record movement paths as time series of x-y-positions at a sampling rate of 12.8 Hz. A recording arena (70×100 cm) with three pellet feeders and one water-outlet in the corners was positioned in a custom-made recording box equipped with foamed plastic that provided light and acoustic insulation. Recordings took place under constant darkness. We analyzed locomotor behavior by applying algorithms developed to analyze open-field locomotion in rodents [34]. Speed values (cm/s) were calculated on position time series with a moving window of 0.3 s. Separation of rest vs. motion episodes was based on a noise level of 4 cm/s. Using smoothed histograms of logarithmic maximal speed derivative values (log max-SD) we

identified two different natural modes of motion in control and PD rats. We further calculated descriptive statistical parameters, i.e., spatial spread (cm) and average max-SD (cm/s), on episodes of full motion to assess the hypo- and bradykinetic state of PD rats and to compare it with control animals.

Electrophysiology

To assess oscillatory activity along the cortex-STN axis in awake and unrestrained animals during quiet rest approximately 14 days after lead implantation we recorded LFP from STN leads (tip impedance 80–120 k Ω , ring \sim 1 k Ω) and ECoG signals from screws implanted above the frontal cortex (see Figure 1). Signals were referenced against nasal and cerebellar screws, pre-amplified, amplified, A/C-coupled and bandpass filtered (1–100 Hz, multi-channel processor, Alpha Omega) and recorded with a sampling rate of 1 kHz (Spike 2). We performed subsequent offline processing steps with routines written in MATLAB (The Mathworks, Natick, USA). These included creation of bipolar derivations of STN-LFP signals and digital notch filtering to remove 50 Hz line noise. Power spectra of LFP and ECoG signals across data epochs of 10–20 min length were calculated using Welch's method as implemented in MATLAB. For statistical comparisons we normalized the power spectrum density (PSD) to the total power between 1–80 Hz. For illustration purposes we first multiplied power values with the corresponding frequency and then normalized the resulting values to the total power in time-frequency plots to account for the 1/f decay of spectral power. We assessed statistically significant power differences between PD rats and controls within seven frequency bands (delta 1–3 Hz, theta 4–7 Hz, alpha 8–12 Hz, low beta 13–24 Hz, high beta 25–35 Hz, low gamma 36–49 Hz, high gamma 51–80 Hz) using the non-parametric Wilcoxon rank sum test ($P < 0.007$, Bonferroni-corrected for seven frequency bands).

High-Frequency-Stimulation

At 18 ± 5 days after electrode implantation (see Figure 1), individual animals received continuous unilateral STN-HFS for 23 hours. Awake rats were placed in the monitoring box and stimulation leads were fed out via an electric slip ring allowing free rotation of cables, thus ensuring unrestrained stimulation and monitoring conditions. To generate stimulation, we used a constant current source (Otoconsult, Frankfurt, Germany) with driving input from a waveform generator (Tektronix, Beaverton, USA) and monitored the output stimulus waveform using a digital oscilloscope (Fluke, Glottertal, Germany). HFS-parameters were adapted for safe and chronic application in rodents [31,32,35]. Cathodic, bipolar, charge-balanced pulses of 60 μ s pulse-width, 130 Hz stimulation frequency and 300 μ A current amplitude were applied. We controlled for the current spread to adjacent neuronal structures by carefully monitoring stimulation-induced behavioral responses. As such, dyskinetic movements of the contralateral paw, face or rotational behavior were observed upon a stepwise current increase, consistent with previously reported side effects of stimulation in the subthalamic area [31,36]. The current amplitude for subthreshold HFS was then set at 300 μ A, a value approximately 30% below the threshold for stimulation-induced side effects (450 ± 50 μ A, median \pm MAD).

Tissue sampling

Immediately after STN-HFS, we induced deep anesthesia with isoflurane followed by i.p.-injection of ketamine (100 mg/kg) and xylazine (6 mg/kg). The time between induction of anesthesia and tissue isolation was crucial with respect to the effect of biological RNA degeneration and the effect of anesthesia itself. We perfused

animals transcardially via the ascending aorta with ice-cold saline solution (0.9% NaCl, 10,000 IU heparin added for anti-coagulation; B. Braun) and rapidly removed the brain under ongoing perfusion, thereby cooling down the whole animal body within 5 minutes after induction of anesthesia. The brain was then transferred to a brain slicing matrix (David Kopf Instruments) to cut out a coronal slice ranging from -3 to -6 mm relative to the frontal apex. From this slice, three tissue samples from motor cortical areas M1-2 and S1 of both hemispheres were manually dissected with a sample corer (2 mm diameter; WPI, Sarasota, USA). Probes were immediately flash-frozen in liquid nitrogen and stored at -80°C for mRNA extraction. The second tissue block containing STN, VTA and SNc was immersion-fixed in 4%-PFA-solution (paraformaldehyde in 0.1 M phosphate buffered saline, Sigma-Aldrich) for subsequent histological analysis. In total, the whole procedure lasted less than 15 minutes. Regarding RNA degradation, assessment on the BioAnalyzer-platform (Agilent Technologies, Santa Clara, USA) revealed good quality and high purity of all RNA samples (A_{260}/A_{280} -ratios 2.06 ± 0.04 ; data not shown). Brains were removed under ongoing perfusion in an attempt to elaborate the washout process and minimize sample contamination with systemically active anesthetics. Nevertheless, given the fact that other studies showed significant alteration of gene expression after brief exposure of the brain to central anesthetics (ketamine [37] and gamma-hydroxybutyrate [38]), we cannot completely exclude a possible bias.

Counting of TH-positive cells in the SNc and VTA

To evaluate dopaminergic cell loss in PD rats and controls we performed free-floating tyrosine-hydroxylase (TH) immunohistochemistry on serial 40 μ m coronal sections of the midbrain. The immersion-fixed tissue block containing the SNc was transferred to 30%-sucrose solution and kept at 4°C for 24 hours. Sections were cut with a freezing-microtome (Leica Instruments, Wetzlar, Germany) and stained in free-floating fashion for TH-activity. Briefly, sections were washed in phosphate buffer (0.01 M PBS, Sigma-Aldrich), incubated with 3%- H_2O_2 -solution for three minutes to block endogenous peroxidase activity and incubated with 2% normal horse serum (added with 0.3% Triton X-100, Sigma-Aldrich) for 30 minutes. Sections were then incubated overnight at 4°C with the primary TH-antibody (1:250, monoclonal mouse antibody, Novocastra reagents, Leica Microsystems, Wetzlar, Germany), followed by the biotinylated secondary antibody (1:400, Novocastra reagents) for 30 minutes, and afterwards incubated with avidin and biotinylated horseradish peroxidase (ABC kit, Novocastra reagents) for another 30 minutes. TH was visualized by adding peroxidase substrate (0.02% DAB reagent in 0.003% H_2O_2 in PBS) for 2 to 10 minutes duration. Finally, sections were mounted on glass slides, dehydrated in an increasing alcohol row and fixed under a cover slid with Roti Histokitt II (Carl Roth, Karlsruhe, Germany).

Unbiased stereological counting of TH-positive cells in the SNc and VTA was performed using StereoInvestigator 10.0 Software (MicroBrightField Inc., Williston, Vermont, USA) mounted to an Olympus Bx61 brightfield microscope (Olympus Deutschland GmbH, Hamburg, Germany) equipped with a Microfire TM A/R camera (Optronics, California, USA) and an x-y-z galvanometer (Carl Zeiss AG, Jena, Germany). The optical fractionator probe [39,40] was applied on series of 40 μ m thick coronal sections. Technical restrictions (preservation of material for molecular processing) did not allow the analysis of the total volume of SN and VTA. In order to sample comparable parts of the SN and VTA, the stereological analysis was centered on an independent anatomical landmark, chosen as the rootlets of the oculomotor

cranial nerve. Overall we sampled six sections (sampling rate of three sections), thereby spanning 600 μm in the cranio-caudal dimension. However, due to availability of continuous TH-sections containing SNc and VTA, two animals were investigated using sampling rates of two and six sections, respectively. Using a 2,5x lens with NA 0.075 we defined three anatomical regions of interest (ROI), i.e., the substantia nigra pars compacta (SNc), substantia nigra pars reticulata (SNr) and ventral tegmental area (VTA) [30]. For anatomical 3-D reconstructions of ROIs and counted cells see Figure S1. Cell counting was performed using a 40x Plan-Neofluar dry type objective lens with NA 0.75 (Carl Zeiss AG) within the SNc and VTA-ROIs. The counting frame (50 \times 50 μm) with a dissector height of 20 μm was applied with a uniform random sampling grid of 150 \times 150 μm (optical dissector volume of 50000 μm^3 , sampling grid area of 22500 μm^2 , [41]). Schmitz-Hof's second coefficient of error ranged between 0.1 and 0.15 for the VTA of both controls and PD animals, as well as the SNc of controls. For SNc-ROIs of PD animals it ranged between 0.4 and 0.8, thus reflecting the scarceness of TH-positive cells [40,41]. The total volume of the sampled SNc and VTA parts was stereologically estimated using the Cavalieri method [42]. As our histological regime did not allow sampling the whole SNc and VTA in the cranio-caudal dimension, we expressed TH-positive cell numbers as cell density (cell count/ mm^3) within the sampled volume. Cell densities were calculated for each ROI and hemisphere and then averaged across hemispheres (n=6 hemispheres per group). We used non-parametric statistical measures for comparing TH-positive cell depletion between PD and control animals (Wilcoxon rank sum test).

Verification of Electrode Placement and Stimulation Induced Tissue Damage

Placement of electrode leads and the surrounding tissue damage was verified in photomicrographs of serial 40 μm coronal brain sections, cut as described above and stained with cresyl-violet (Nissl 5%-solution, in acetate buffer of pH 3.8–4.0). Sections were mounted on glass slides and incubated with Nissl solution until the desired staining intensity was obtained. Afterwards, sections were clarified in chloroform containing solution, degreased in successively increasing alcohol concentration and fixed as described above for TH-sections. We considered the placement of electrodes as correct only if the electrode tract hit the STN in three consecutive sections. The tissue response to electrode placement and stimulation-induced damage was analyzed in the section showing greatest tissue reaction [43]. The area infiltrated with mononuclear cells (MNC) as defined under light microscopy was determined using commercial image-analyzing software (AxioVision, Carl Zeiss) and compared between pulsed and unpulsed electrodes for statistically significant differences using the non-parametric Wilcoxon rank sum test. MNC are known to infiltrate the sheath of tissue surrounding also unpulsed electrodes [44]. Furthermore, sections were checked for signs of neuronal damage by electrical lesions (i.e., coagulation).

Gene Expression Profiling

Total RNA was extracted from tissue samples of six STN-HFS treated rats (PD n=3, control n=3) using the RNeasy Lipid Tissue Mini Kit (Qiagen, Hilden, Germany), which purifies all RNA molecules longer than 200 nucleotides providing enrichment for mRNA. After quality assessment of RNA (BioAnalyzer-platform, Agilent Technologies, Santa Clara, USA), we analyzed 4 μg RNA extract of two PD and two control rats on Affymetrix Rat Expression 230 2.0 chips (Affymetrix, Santa Clara, USA) as described previously [45]. This required cDNA synthesis, labeling

and hybridization according to the protocol of the manufacturer (Affymetrix GeneChip Expression Analysis Technical Manual). Following incubation in the Affymetrix Hybridization Oven 640 at 45°C for 16 h, gene chips were washed and stained using the Affymetrix Fluidics Station 450. We scanned microarrays with the Affymetrix GeneChip Scanner 7G, and processed the signals using GCOS (V1.4, Affymetrix) and Expression Console (V1.1, Affymetrix) software. Chips were scaled to a target value of 300 and normalized using robust multiarray averaging (RMA). We requested uniform quality of MA experiments assessed on the basis of the number of present probe sets, RMA signal histograms, unsupervised hierarchical clustering and Pearson's correlation matrix of RMA signals. To reduce the influence of systematic noise caused by, e.g., circadian rhythmicity [46] or the behavioral state of the animal [47], our protocol utilized an intra-animal contrast of gene regulation. The first analysis specifically addressed the HFS-effect and incorporated four comparisons of stimulated vs. non-stimulated hemispheres (two intra-animal and two inter-animal cross-comparisons). We generated gene regulation lists with the 'change p value algorithm' of the GCOS software package (Affymetrix) which provides change calls on the basis of paired t-tests between corresponding probe sets (n=31043, Affymetrix Rat Expression 230 2.0). To account for the low number of biological microarray replications we requested from a candidate gene to show equal regulation calls in all four comparisons. In our second analysis, we addressed the gene expression changes that constituted the baseline of our first analysis and may reflect 6-OHDA related changes. To this end, the non-stimulated hemispheres of PD vs. those of control animals were analyzed for homonymous change calls. Regulated transcripts were filtered with a signal-log ratio (slr) threshold of ± 0.6 (i.e., the base 2 logarithm of a 1.5 fold-change) for all individual comparisons. Regulation lists were analyzed for functional enrichment of Gene Ontology (GO)-terms and KEGG (Kyoto Encyclopedia of Genes and Genomes) pathways using the DAVID database for annotation, visualization and integrated discovery [48,49] (<http://david.abcc.ncifcrf.gov>).

Real-time RT-PCR analysis

To validate microarray expression profiling for selected genes, real-time RT-PCR analysis was performed as described previously [50]. We report data from validated TaqMan-Gene expression assays for RT1-Da (Rn01427980_m1), Cd74 (Rn00565062_m1), Rasgrp2 (Rn00570056_m1) and Rpl13a (Rn00821946_g1). Four additional genes from a less strict generation of regulation lists (i.e., 2/4 change count, intra-animal comparisons; Gabra3, Glra2, Nxp3 and Syt4) were investigated for exploratory reasons (data not shown). All genes were investigated in triplets. The relative expression of target mRNA was normalized to the housekeeping gene Rpl13A. Change calls were expressed with the $\Delta\Delta\text{CT}$ -method (i.e., the base 2 logarithm of the fold change and equals the slr). Within and across group statistical comparisons utilized the non-parametric Wilcoxon rank sum test (fixed effect analysis, $P < 0.007$, Bonferroni-corrected for seven investigated genes).

Western blot analysis

Proteins were purified from the phenolic phase of the RNeasy Lipid Tissue Mini Kit (Qiagen) as up to 98% of total protein can be solubilized from TRIzol treated samples [51]. To this end the phenolic phase was incubated with 1,5 ml isopropanol (Sigma-Aldrich) for 10 min at room temperature. After centrifugation (11500 x g, 4°C) the pellet was washed three times with 2 ml guanidiniumhydrochlorid solution (0.3 M in 95% ethanol; Sigma-Aldrich) at room temperature for 20 min each and spun down

(4500 × g, 4°C). Finally, the pellet was washed 20 min with 2 ml ethanol (100%, Sigma-Aldrich) at room temperature and air-dried after centrifugation. Protein pellets were solubilized in 200 µl reducing protein solubilizing buffer (Machery-Nagel, Düren, Germany), boiled for 10 minutes, centrifuged and supernatants were stored at -20°C for further usage. Western blotting was carried out essentially as described previously [50]. We used polyclonal antibodies against CD74 (C-16; goat-antiserum; dilution 1:500), RT1-D (OX-17; mouse-antiserum; dilution 1:200) and RT1-B (HIS-19; mouse-antiserum; dilution 1:200), from Santa Cruz Biotechnology Inc. (Heidelberg, Germany). Additionally, we used two antibodies to detect the astroglial marker GFAP (GA-5; mouse-antiserum; dilution 1:1000) and the microglial and macrophage marker Iba-1 (C20; goat-antiserum; dilution 1:1000). Bound antibody was stained using goat anti-mouse, goat anti-rabbit or rabbit anti-goat secondary antibodies conjugated with horseradish peroxidase (Jackson Immuno Research Europe Ltd., Suffolk, UK) and visualized using enhanced chemiluminescence substrate (Pierce Protein Biology Products, Thermo Scientific, Bonn, Germany). X-ray films of Western blots were scanned and protein bands were quantified by densitometry using an ImageJ plugin (Version 1.46, NIH, USA).

Statistical analysis

Throughout the paper, we utilized non-parametric statistical measures to check for significant differences between PD and control animals (Wilcoxon rank sum test). However, generation of regulation lists using GCOS (Affymetrix) applied paired t-tests between corresponding probe sets, as implemented in the software package. Statistical results are presented as mean ± standard deviation (SD) unless stated otherwise. The alpha level of <0.05 was corrected for multiple comparisons using Bonferroni's method in case of power-spectral and RT-PCR analyses.

Results

Verification of HFS electrode placement and tissue reaction

Microelectrode-guided targeting of the STN led to a high rate of successfully implanted STN-HFS electrodes in rats used for gene expression profiling (n = 6; for a typical electrode trajectory, see Figure 2A). In 10/12 implanted hemispheres we detected a hit of the STN in at least three consecutive sections. One control rat was implanted approximately 250 µm anterior to the rostral margin of the STN. However, as the threshold for inducing typical dyskinetic movements in this animal did not differ from the group average, it was still included in confirmatory RT-PCR validation. Stimulated and non-stimulated hemispheres exhibited mild MNC infiltration, which was expected as a reaction to the electrode implantation itself [44] (see Figure 2B). Non-parametric statistical comparison revealed a trend but no significant difference between pulsed and unpulsed electrodes (MNC infiltrated area around pulsed electrode tips: $1.79 \pm 0.3 \times 10^5 \mu\text{m}^2$ vs. $1.14 \pm 0.7 \times 10^5 \mu\text{m}^2$ around unpulsed tips; mean ± SD, P = 0.065, Figure 2C). Additionally, two stimulated hemispheres (1 PD, 1 control) showed small areas of coagulation (1.3 and $1.7 \times 10^5 \mu\text{m}^2$). Cortical tissue from those animals was not used for microarray screening, but included in confirmatory RT-PCR analysis.

Stereological quantification of TH-positive cells

Bilateral injections of 15 µg 6-OHDA into the SNc resulted in extensive cell death of dopaminergic neurons in the SNc approximately 14 weeks after neurotoxin injections (see Figure 3A-F for representative photomicrographs of the midbrain at

approximately -5.5 mm relative to Bregma of one control and one PD rat; see Figure S1 for 3-D reconstructions of stereological results). The cell density of nigral TH-positive neurons was reduced by -94% in PD animals compared to controls (532.3 ± 672.9 cells/mm³ in PD vs. 8675.6 ± 2374.5 cells/mm³ in controls; P = 0.002; Wilcoxon rank sum test; see Figure 3G). VTA neurons exhibited no significant depletion (9084.4 ± 4441.3 cells/mm³ in PD vs. 12156 ± 2233 cells/mm³ in controls, -25.3%, P = 0.3; see Figure 3G). Comparison of depletion values between single hemispheres yielded similar values for both hemispheres except for one PD animal that showed depletion of VTA dopaminergic neurons in the right hemisphere (data not shown). The cell density of SNc neurons of vehicle injected rats was comparable to numbers of TH-positive cells reported by a previous study [52] that carried out investigations in Fisher 344XBrown Norway hybrids. Other studies reported significantly higher values in different rat strains (Lewis rats [53], Long-Evans rats [54], Sprague-Dawley rats [55]), which suggests large differences in the absolute number of mesolimbic dopaminergic cells in different rat strains.

Behavioral monitoring revealed hypo- and bradykinetic state

Upon visual inspection, spontaneous locomotion and movement speed of 6-OHDA-injected rats appeared reduced and body posture revealed a hunchback-like shape. Hind limb rigidity was detectable upon manual assessment. PD rats displayed anorexia and adipsia to a variable degree, leading to an average postoperative weight loss of $17.2 \pm 9.2\%$ vs. $1.1 \pm 3.7\%$ (mean ± SD) in controls prior to behavioral monitoring (P = 0.13). No control rat showed overt bradykinesia, anorexia or adipsia. Nine of twelve PD rats stabilized weight loss within 14 days after SNc surgery. No additional signs of altered animal behavior that could indicate persistent pain distress, e.g., vocalization upon gentle palpation or mutilation such as licking, biting, scratching or other form of harming body parts was detected during daily inspections. In synopsis of all clinical features we interpreted the presented behavior as a pronounced parkinsonian phenotype following bilateral 6-OHDA injections into the SNc.

Quantitative assessment of the absolute spatial spread and the maximal speed derivative (max-SD) obtained from episodes of full blown motion confirmed the reduced locomotor activity of PD vs. control rats included in gene expression experiments. Figure 4A-B shows examples of raw movement tracks of one control (A) and one PD animal (B) at the different time points of behavioral monitoring. Postoperatively, the spatial spread was decreased on average to 81.3 ± 28.4 m in PD rats vs. 142 ± 27 m in controls (see Figure 4C). The max-SD was reduced to 17 ± 0.7 cm/s in PD rats vs. 20.5 ± 1.8 cm/s in controls (see Figure 4D). Compared to preoperative values, PD rats showed a relative reduction of -35.7% for spatial spread and -14.6% for max-SD in contrast to -6.2% for spatial spread and -4.3% for max-SD of controls. Note that spatial spread and max-SD values of rats included in gene expression experiments were placed well within the group variance at pre- and postoperative recording times (n = 9 PD and n = 8 controls, data not shown). However, the obtained pre- and postoperative behavioral estimates did not differ significantly in a non-parametric statistical comparison (P = 0.1 for PD pre vs. postoperative; P = 1 for controls pre vs. postoperative; n = 3 PD and n = 3 controls).

To assess the reversal of experimental parkinsonism by 23h of unilateral STN-HFS, we monitored PD and control rats before (cables attached, no stimulation) and during 130 Hz stimulation. Notably, STN-HFS in PD rats led to an increase of 18.9% in

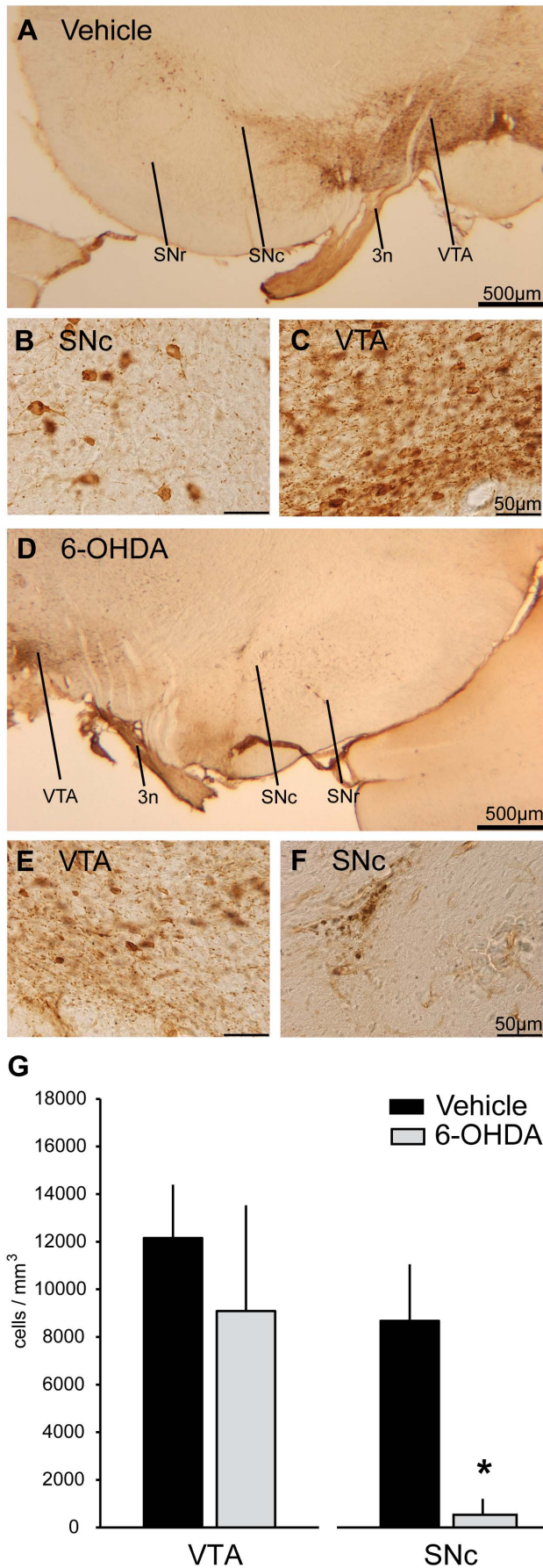


Figure 3. Stereology of tyrosine-hydroxylase positive midbrain neurons. Representative sections (2,5x lens) of the midbrain depicting the rootlets of the third oculomotor cranial nerve (3n), VTA, SNc and SNr stained for tyrosine-hydroxylase (TH) of an example control (A) and example PD rat (D). Photomicrographs show magnifications taken with a 40x lens and depict TH-positive dopaminergic cells in the SNc (B) and VTA (C) of a vehicle injected rat, as well as of a 6-OHDA injected rat (E and F, respectively). Results of unbiased stereological cell counting (G) are presented as estimated cell density (mean ± SD cells/mm³) for the VTA and SNc of all rats included in gene expression profiling (n = 3 PD, n = 3 control). Filled black bars indicate cell estimates respectively of vehicle and gray filled bars of 6-OHDA injected rats. Statistically significant differences are marked with an asterisk. 3n, 3rd oculomotor cranial nerve; VTA, ventral tegmental area; SNc, substantia nigra pars compacta; SNr, substantia nigra pars reticulata; TH, tyrosine-hydroxylase; 6-OHDA, 6-hydroxydopamine. doi:10.1371/journal.pone.0091663.g003

spatial spread compared to cable attached monitoring in the absence of stimulation. In contrast, control animals showed a decrease of -26.7% in response to STN-HFS (see trend in Figure 4C-D). Although observable in raw movement tracks (Figure 4A-B, middle-right and right inserts) these trends likewise did not reach statistical significance. The max-SD showed a mild and

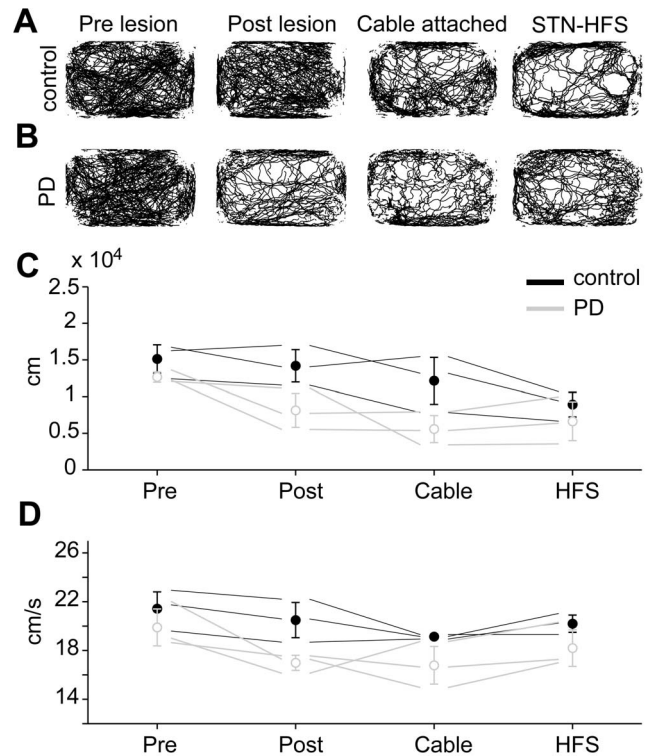


Figure 4. Spontaneous locomotor activity revealed parkinsonian phenotype. The upper row (A) depicts spontaneous 23h locomotor activity of a representative control rat, the lower row (B) of an example PD rat. Recordings were performed before (left) and after 6-OHDA or vehicle injections (left-middle) as well as before (right-middle) and during unilateral STN-HFS (right). The lower row depicts descriptive statistics of spatial spread (C) and maximal movement speed derivative (max-SD; D) averaged over episodes of full blown motion for all four recording times (see above). Markers and error-bars indicate the mean ± SD of animals included in gene expression profiling (n = 3 each group; controls filled-black, PD rats open-gray symbols). Thin lines indicate each single animal included in gene expression profiling. PD, Parkinsons disease; 6-OHDA, 6-hydroxydopamine; STN, subthalamic nucleus; HFS, high-frequency stimulation. doi:10.1371/journal.pone.0091663.g004

non-significant increase of 8.5% in PD and 5.5% in control rats due to STN-HFS.

Pronounced oscillatory activity in STN- and ECoG-LFPs

Oscillatory activity in the 30–40 Hz-frequency range was clearly observable in monopolar frontal cortex ECoG and bipolar STN-LFP recordings in PD rats (6/6 and 3/6 hemispheres, respectively), but not in controls (0/6 and 0/6, respectively). Figure 5A depicts short epochs of raw STN-LFP (upper row) and frontal cortex ECoG (lower row) data recorded in PD rats (right column) and controls (left column) during quiet rest. Figure 5B shows time-frequency plots of LFP- and ECoG-power of all PD animals included in gene expression profiling. We saw marked oscillatory activity in the STN of 3/6 PD-hemispheres and chose the side of HFS accordingly, taking into account that oscillatory strength and extent of the oscillatory region in PD patients correlates with DBS-efficacy [56]. We calculated grand average power spectra (Figure 5C) by pooling data across all hemispheres of all animals included in gene expression profiling and, in case of STN-LFPs, by pooling separately across hemispheres ipsi- and contralateral to HFS electrodes. We compared the relative power in seven different frequency bands between PD rats and controls using non-parametric statistics (significant frequency bands are labeled with an asterisk in Figure 5Ci-v; $P < 0.007$, Bonferroni-corrected for seven frequency bands). In ECoG recordings, relative power in the high beta/low gamma band (25–34 Hz) was significantly increased in PD rats compared to controls (Figure 5Ci). A less broad but similarly distinct and significant peak was visible in the grand average of STN-LFPs (Figure 5Ciii) ipsilateral to subsequent HFS. No peak was visible on the contralateral side (Figure 5Civ). At the same time, relative power in the gamma range (35–47 and 51–80 Hz) was significantly decreased in PD vs. controls. This decrease in gamma-power was most pronounced in STN-LFPs (Figure 5Cv), but also present in ECoGs (Figure 5Cii) recorded from PD rats.

STN-HFS induced changes in sensorimotor cortical gene expression

STN-HFS led to downregulation of six genes in PD rats showing homonymous regulation in both intra- and across-animal comparisons (see Table 1). Five genes encoded major histocompatibility complex (MHC) class II proteins (i.e., RT1 class II, locus Ba with three transcripts, locus Bb, locus Da and locus Db1, Cd74 antigen) and one gene encoded an MHC-class I protein (RT1 class I, CE5). These genes comprised a significantly enriched cluster of ‘Antigen processing and presentation of peptide antigen’ related genes (EASE = 5.3; the EASE-score is the minus log transformation of annotation P-values, [40]). Furthermore, they also constituted the members of ten significantly enriched KEGG-pathway, e.g., ‘Antigen processing and presentation’ and ‘Cell adhesion molecules (CAMs)’. Along with MHC genes the Complement factor 2 gene (C2) was downregulated in three of four comparisons, enlarging the group of immune response genes in our data set. Notably, none of these immune response genes was regulated by STN-HFS in vehicle injected controls.

All MHC class II genes, but not the MHC class I gene or C2, were found upregulated in 6-OHDA lesioned rats (lesion effect analysis). That is, the slr-change direction due to STN-HFS was opposite to the slr-change direction of the lesion effect comparison. Hence, increased expression of MHC class II genes observed in parkinsonian rats following 6-OHDA lesioning was reversed by STN-HFS (see Table S1). We termed this effect ‘counter-regulation’.

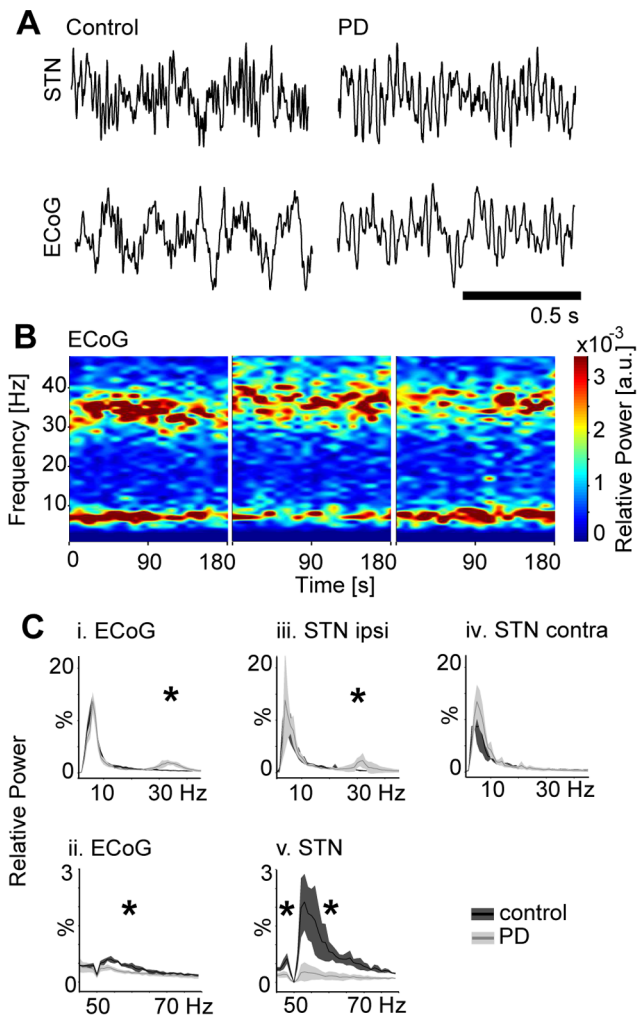


Figure 5. Spectral analysis of cortical and subthalamic local field potentials. Representative examples (A) of oscillatory activity in the raw local field potentials (LFP) recorded from STN (upper row) and frontal ECoG (lower row) of controls (left column) and 6-OHDA treated parkinsonian rats (right column). Time-frequency plots (B) of spectral power during 180 s of quiet rest from all PD animals included in gene expression analyses. Power spectra (C) calculated from frontal ECoG and STN-LFP data of parkinsonian rats (light gray lines/shadings) and controls (dark gray lines/shadings): (i) low-frequency range (1–45 Hz) and (ii) high-frequency range (45–80 Hz) of ECoG-power spectra pooled across all hemispheres ($n = 6$). (iii) Low-frequency power spectrum of STN-LFP ipsilateral to the side of HFS and (iv) contralateral to the side of HFS ($n = 3$ each). (v) High-frequency power spectrum of STN-LFP pooled across all hemispheres. Asterisks indicate significantly different frequency bands. Note the dampening at 50 Hz that resulted from bandpass filtering of line noise. LFP, local field potential; STN, subthalamic nucleus; ECoG, electrocorticogram; 6-OHDA, 6-hydroxydopamine, HFS, high-frequency stimulation. doi:10.1371/journal.pone.0091663.g005

Microarray confirmation with RT-PCR and Western blotting

RT-PCR analysis and Western blotting were based on samples from a total of three 6-OHDA and three vehicle injected animals (i.e., aliquots of the same two samples per group that had been used for microarray experiments plus RNA isolated from an additional animal per group). MHC class II genes Cd74 and RT1-Da showed significant homonymous downregulation in RT-PCR analysis, not only confirming microarray results but also revealing

Table 1. STN-HFS regulated MHC genes in sensorimotor cortex.

Gene Title	Gene Symbol	Probe Set ID	STN-HFS effect in 6-OHDA group			STN-HFS effect in vehicle group			Lesion effect		
			D-count	I-count	slr	D-count	I-count	slr	D-count	I-count	slr
RT1 class II, locus Da	RT1-Da	1370883_at	4	0	-2.7	0	0	—	0	4	1.5
RT1 class II, locus Db1	RT1-Db1	1370383_s_at	4	0	-2.7	1	1	—	0	4	1.9
RT1 class II, locus Bb	RT1-Bb	1371033_at	4	0	-2.6	1	0	—	0	4	1.5
CD74 antigen	Cd74	1367679_at	4	0	-2.4	0	0	—	0	3	1.2
RT1 class II, locus Ba	RT1-Ba	1381593_x_at	4	0	-2.4	0	0	—	0	4	1.2
RT1 class II, locus Ba	RT1-Ba	1392334_at	4	0	-2.2	0	0	—	0	4	1.3
RT1 class II, locus Ba	RT1-Ba	1370822_at	4	0	-1.6	0	0	—	0	4	1
RT1 class I, CE5	RT1-CE5	1388255_x_at	4	0	-1.4	1	0	—	0	0	—

List of all microarray regulated genes exceeding the slr-threshold of ± 0.6 and showing homonymous regulation in both intra- and across-subject comparisons. Gene name, gene symbol and Affymetrix ID are given with the respective decrease (D) or increase (I) count as well as the mean slr. Data are presented for 6-OHDA and vehicle treated rats and for the effect of lesion analysis that compared the gene expression change between the non-stimulated hemispheres of 6-OHDA and control rats. Slr, signal-log ratio; 6-OHDA, 6-hydroxydopamine. doi:10.1371/journal.pone.0091663.t001

a similar strength of expression changes in RT-PCR (see Figure 6A-B). Comparable to the microarray lesion effect analysis, Cd74 and RT1-Da showed upregulation by 6-OHDA injections in confirmative RT-PCR comparisons of the non-stimulated hemispheres (Figure 6C).

Western blotting revealed that the MHC class II protein RT1-D showed downregulation by STN-HFS in all investigated PD rats (see Figure S2). CD74 showed downregulation on the protein level

in both PD rats that were investigated with microarrays but not in the third PD rat that had received STN-HFS and was added for confirmatory analyses. For RT1-B, another MHC class II member, we did not observe STN-HFS induced downregulation on the protein level as suggested by microarray analysis. Vehicle injected control animals showed no regulation on the genetic level and no consistent regulation pattern on the protein level due to STN-HFS. To investigate whether the changes in immunity-related genes and proteins were associated with an altered state of activity in astrocytes or abundance of microglial cells or macrophages we additionally investigated the protein levels of GFAP and Iba-1, respectively. GFAP protein regulation resembled the protein regulation pattern of CD74 in both 6-OHDA-lesioned and control animals (see Figure S2 and S3). In contrast, only low levels of Iba-1 protein could be detected without revealing a distinct regulation pattern.

Discussion

Dopamine depletion in PD leads to a wide range of pathological alterations of the cortico-basal ganglia network, ranging from gene expression to network synchrony that ultimately lead to motor symptoms. The therapeutic effects of STN-HFS on different motor symptoms occur at variable latencies, which likely reflects the multiple effects on these different levels of organization. Here we examined HFS-induced changes in gene expression in control and 6-OHDA lesioned animals displaying the behavioral phenotype and electrophysiological signatures of PD. The results suggest that the expression of MHC class II genes in sensorimotor cortex is increased by dopamine depletion and returned to baseline levels by STN-HFS. Understanding the complex interplay of MHC genes in PD might eventually help to understand the neural mechanisms underlying the therapeutic mechanism of STN-HFS in this debilitating disease.

Technical considerations

We chose to apply a whole genome analysis in order to identify genes regulated by STN-HFS in tissue samples taken from rat sensorimotor cortex, as this cortical area is a major source of “hyperdirect” cortico-STN afferents, the importance of which has repeatedly been highlighted in attempts to explain the therapeutic

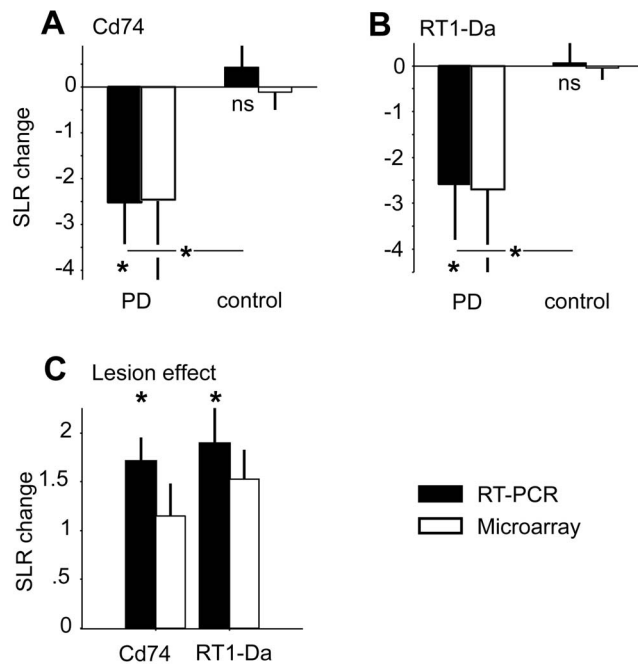


Figure 6. Real-time RT-PCR. Real-time RT-PCR results for MHC class II genes Cd74 (A) and RT1-Da (B) regulated by unilateral STN-HFS. Lesion effect comparison (C) for both MHC class II genes. Filled black bars indicate signal-log changes of RT-PCR analysis and open bars the results of microarray experiments (mean \pm SD). Asterisks denote statistically significant results. MHC, major histocompatibility complex; STN, subthalamic nucleus; HFS, high-frequency stimulation. doi:10.1371/journal.pone.0091663.g006

effects of STN-HFS [16,17,22]. We deliberately chose to investigate HFS-effects in brain tissue that did not receive direct electrical stimulation, avoiding contamination due to tissue reaction or damage following direct electrical manipulation.

We utilized an intra-animal contrast, comparing stimulated and non-stimulated hemispheres within the same animal. Bearing in mind the almost infinite endogenous and exogenous factors having an effect on gene expression this represents a viable biological control. It is impossible to create exactly the same test conditions for different animals with respect to, e.g., circadian rhythm, diet, light, noise or handling. In fact, a large set of genes (approximately 1–10% of all present transcripts in brain or liver tissue) is known to oscillate in a circadian manner [46] or is influenced by the behavioral state and vigilance of the animal [47]. These circumstances would lead to unspecific noise in an across-animal experimental design with the potential to obscure small but biologically relevant changes in STN-HFS related gene expression. The intra-animal contrast is robust against such factors, as global influences on gene expression should influence both hemispheres similarly and would filter out as a result of the differential analysis. On a behavioral level, unilateral STN-HFS did not alter the motor performance of PD animals with statistical significance. Nonetheless, a trend for normalized spatial spread and movement speed was observed. Interestingly there is also clinical evidence for a bilateral motor benefit in PD patients treated by unilateral STN-HFS [57–59]. However, compared to the pronounced and persistent contralateral effects typically observed with STN-HFS, ipsilateral benefits are much smaller and show a marked attenuation over time. A recent study [17] investigating STN-HFS evoked cortical potentials only found a small effect in the contralateral hemisphere following stimulation with 60Hz, but not 130Hz, the frequency used in the present study. Consistent with this finding, we did not observe induction of immediate early genes in the contralateral hemisphere after unilateral 130 Hz STN-HFS in a previous study [23]. Taken together, the complex reorganization of cortico-basal ganglia network structures and -functioning will likely involve both ipsi- and contralateral effects of unilateral stimulation. With our experimental design, we can detect genes that exhibit a differential regulation with a high sensitivity but would under appreciate or miss out bilaterally regulated genes. Furthermore, we could underestimate the regulation strength of unequally regulated genes. Thus, to obtain a complete and unbiased perspective on gene regulation under STN-HFS, follow-up experiments that utilize the across-animal comparison with an implanted but not stimulated group of controls would be necessary.

General anesthesia itself alters gene expression in the brain [37,60], and is a strong modulator of neuronal activity in subcortical structures [61] or of cortical connectivity and network states [38]. Such vigilance-dependent modulation might interfere with the genomic baseline, possibly masking relevant changes induced by STN-HFS. Whereas STN-HFS was applied to the freely moving animal, tissue harvesting took place after brief induction of anesthesia. Although dose-dependent effects of centrally active anesthetics may have been ameliorated by the immediate perfusion with ice-cold saline, we cannot exclude a possible bias. However, as the contralateral side to stimulation served as an internal control, bilateral effects of anesthesia could filter out in our experimental design.

Studies addressing HFS-regulated gene expression often utilize acute stimulation regimes of up to 3 hours. A chronic animal model enables longer stimulation times and allows for a behavioral assessment of stimulation effects and efficacy. We chose an intermediate stimulation time of 23 hours in order to identify

genes that are up- or downregulated after an initial phase of immediate early gene induction and are possibly involved in adaptive processes.

Histological analyses revealed mild infiltration of mononuclear cells around both pulsed and unpulsed electrode tips as well as two small electrical lesions in one PD and control rat each. Though distant to the sensorimotor cortex, STN lesions may still bias cortical gene expression. To minimize the rate of false positive genes we excluded the respective samples in exploratory microarray analyses. Thus, minor electrical lesions would not bias the hypothesis that a found candidate gene is regulated by STN-HFS in a biologically meaningful way. In this respect, the homonymous regulation of several genes from a certain gene network represents an immanent biological control.

In order to have matched control hemispheres we used bilaterally lesioned animals, which resemble more closely the extent of dopamine loss in most patients compared to hemi-lesioned animals. In our disease model, dopaminergic depletion of the SNc was nearly total (–94% compared to controls), whereas the VTA exhibited no significant cell loss. This dissociation of dopaminergic degeneration is comparable to that seen in humans with PD, where the VTA is significantly less affected than the SN [62]. However, VTA cell loss was more variable and the alteration of the mesolimbic dopamine system in our model could potentially complicate a differentiation between pure parkinsonian motor symptoms (unambiguous loss of movement and bradykinesia) and the extent of motivational deficits leading to apathy, abulia, or anorexia. Nonetheless, human post-mortem studies have estimated 40–50% cell-loss in the VTA [62–66] emphasizing the vulnerability of the mesocorticolimbic dopamine projection in PD. Thus, mesolimbic denervation contributes to the complex clinical phenotype encountered in humans with PD [66], especially in later disease stages.

Spectral fingerprints of PD

Pronounced oscillations with a peak frequency of 32 Hz were observed along the cortico-STN axis of PD rats, along with a severe reduction of power in the gamma-frequency band (45–80 Hz) compared to controls. To the best of our knowledge, this report is the first to demonstrate excessive high beta/low gamma oscillatory activity in the bilateral 6-OHDA rat model. Enhanced beta-oscillations are a widely accepted biomarker reflecting pathological network activity in akinetic-rigid PD patients [67] and animal models of parkinsonism [68]. The observed high beta/low gamma oscillations in our bilateral lesion model resemble oscillations in hemileioned rats [69] and exhibit higher frequencies compared to anesthetized rats (peak frequency of 20 Hz [68]). The observed decreases in gamma-power match results obtained from surgically treated PD patients, in which increased gamma-power in the STN-LFP was observed following dopaminergic medication [70]. Thus, bilateral dopamine depletion led to dramatically altered cortical-subcortical dynamics in our animals. This network dysfunction was associated with the appearance of a parkinsonian phenotype on the behavioral level.

Protein expression of selected candidate genes

We did not find strong similarities between protein abundance and mRNA expression of selected genes (see Figure S3). RT1-D protein levels correlated best with mRNA regulation detected by microarray and RT-PCR analysis. Results for the other genes were more inconsistent and in case of CD74 protein levels were detected for single rats that would not have been predicted from transcript levels. At first glance the weak correlation between mRNA and protein levels may appear surprising. However, this

finding is supported by ample evidence that the correlation between mRNA and protein levels is highly variable and weak. Recent studies showed that only 30–40% of the protein level can be predicted from mRNA transcription [71–75]. Numerous mechanisms regulate the process from transcribing the genetic information until degradation of the protein. This includes mRNA transcription itself, RNA processing (e.g., splicing), RNA stability (half-life differences between transcripts of several hours), influence of regulatory microRNA, regulation of translation (e.g., 3'- and 5'-UTR and other regulatory elements), protein stability (half-life differences from minutes to days) and protein degradation. Therefore there is a weak link between mRNA and protein levels even without taking into account that protein levels alone are bad predictors of protein function in a cellular context. Protein may exist in abundance but may not be fully functional or inactivated (e.g., by phosphorylation, glycosylation and other posttranslational modifications), not translocated to its proper site of action or interacting partners may be missing. Furthermore perturbed systems are more difficult to investigate than steady-state systems, especially when analyzed at a single point in time. For instance, recent upregulation of a given transcript may result in increased protein levels that cannot be detected yet, and vice versa. Similarly, increased transcription may reflect gene induction that was brought about by feedback mechanisms triggered by reduced protein levels. At any rate, RNA synthesis is tightly regulated in cells and depends on a variety of factors. One should keep in mind that mRNA transcription represents the most upstream step and basically the main switch for operating the more or less fixed genetic code. Although proteins bring about phenotypic changes and convey cellular functions, the detection of induced or repressed genes stands for a shift in the currently activated genetic program at the most fundamental level.

STN-HFS decreases cortical MHC gene expression

The cortical expression of MHC class I and II associated genes was strongly decreased by STN-HFS as detected by microarray and RT-PCR analysis. One of these genes, RT1-D, was strongly downregulated on the RNA level and also showed repressed levels of its protein by Western blotting. Notably, rats rendered parkinsonian by the injection of 6-OHDA revealed upregulation of MHC class II, but not class I genes compared to control animals. Thus, the net effect of STN-HFS on MHC class II gene repression in PD rats was ‘normalization’ to expression levels similar to those of non-parkinsonian controls.

MHC class II genes are expressed by reactive microglia and astrocytes [76], and have been linked to the pathology in human PD [77] and PD animal models [78]. Excessive microglial activation is observed in neural structures that undergo neurodegeneration in PD, in particular substantia nigra, striatum, and globus pallidus [77], but also in hippocampus, limbic structures or cortex of parkinsonian brains [79]. In agreement with our findings, MHC class II genes and Complement factor 3 were found upregulated in the basal ganglia of hemi-parkinsonian rats in a microarray screening study [26]. However, three hours of unilateral STN-HFS did not result in downregulation of MHC class II genes in this study, which investigated a block of tissue that included the site of stimulation (STN) and parts of the basal ganglia, but not cortex. Interestingly, HFS of the ventrolateral thalamus was recently reported to upregulate immune-response related genes in the hippocampus of naïve rats [25]. Another report found a similar set of MHC class II genes (RT1-Ba, -Da and Cd74), MHC class I genes and complement factors (e.g., C2, C3) regulated by HFS applied to the dentate gyrus [80]. In this report HFS in awake but not in anesthetized control rats increased

the expression of immune response genes. This suggests that MHC gene regulation, in one way or the other, is altered by electrical high-frequency stimulation of the brain. The change direction, however, would depend on or represent part of the biological consequences of STN-HFS in specific brain structures.

Regarding this, several lines of evidence emphasized the important role that MHC molecules play in neuron-neuron or neuron-glia interactions. MHC class I molecules are involved in synaptic remodeling and establishment of long term potentiation/-depression in the developing neural system [81,82]. Nonetheless there is evidence that MHC class II expression on glial cells may be tightly coupled to neuronal activity [83,84]. In contrast to MHC class I regulation, chronic blockade of neuronal action potentials or of neurotransmitter release increased the expression of MHC class II molecules in microglia. Glutamate administration or stimulation of the p75- receptor with neurotrophins reversed the typical absence of MHC class II expression. Hence, MHC class II expression in microglia is regulated by activity-dependent neuronal mediators and reflects the global activity state of a neural structure [85] in a reciprocal fashion: MHC class II expression appears to rise if physiological neuronal activity is diminished. In this context, upregulation of MHC molecules in 6-OHDA lesioned animals may reflect impaired cortical neurotransmission and decreased levels of cortical activity in parkinsonian animals. In turn, STN-HFS induced MHC class II downregulation would be associated with normalization of cortical activity. The finding of a similar regulation of one MHC class II protein (CD74) and GFAP, an astroglial marker that is upregulated in various pathological states and indicates activated astrocytes, is consistent with this hypothesis. On the other hand, no distinct pattern of Iba-1 regulation could be detected. Hence no excess presence of microglia or macrophages in 6-OHDA treated rats or response to STN-HFS could be shown. In situ studies would be required to determine the effects of STN-HFS on individual cell types in the sensorimotor cortex with respect to transcription and protein expression of MHC-related genes.

Conclusion

Our central finding is that STN-HFS reversed upregulation of MHC class II genes elicited by 6-OHDA lesioning. Thereby it distinctly influences remote sensorimotor cortical areas at a molecular level, giving rise to adaptive changes that may outlast the immediate and short-term effects of STN-HFS. Future research on immunity-related processes and their interplay with STN-HFS may represent a promising perspective on how pathological cortical activity of the Parkinsonian state may be altered and possibly normalized by STN-HFS.

Supporting Information

Figure S1 3-D reconstructions of stereology. Panels (A-F) depict 3D-reconstructions of stereological regions of interest for all 6-OHDA (left column) or vehicle injected rats (right column) used in gene expression profiling. Different ROIs are color-coded (white: left SNr, pale green: left SNc, purple: left VTA, green: right VTA, pale blue: right SNc, cyan: right SNr). Stereological cell counting was only performed in VTA and SNc-ROIs. Spheres indicate stereologically counted cells in the SNc and VTA. 6-OHDA, 6-hydroxydopamine; ROI, region of interest; SNr, substantia nigra pars reticulata; SNc, substantia nigra pars compacta; VTA, ventral tegmental area. (TIF)

Figure S2 Western blot analysis. Detection of MHC class II candidate proteins (RT1-D, RT1-B, CD74), astroglial (GFAP) and microglial (Iba-1) markers by Western blot analysis. All candidates belonged to the enriched gene cluster ‘antigen processing and presentation of peptide antigen.’ The housekeeping protein tubulin served as biological control. All twelve lanes for a given antigen were blotted simultaneously and cropped later for graphical display. 6-OHDA, 6-hydroxydopamine; HFS, high-frequency stimulation; MHC, major histocompatibility complex. (TIF)

Figure S3 Comparison of microarray, RT-PCR and Western blot regulation changes. Quantification of signal-log ratio (slr) changes of MHC class II candidates (RT1-D, RT1-B, CD74), astroglial (GFAP) and microglial (Iba-1) markers. We utilized densitometric quantification to evaluate protein levels in Western blots. No statistical comparison was applied due to low sample size and missing data regarding RT-PCR (RT1-B, GFAP and Iba-1 were only investigated by Western blotting). (TIF)

Table S1 Microarray expression values MHC class II genes. RMA-normalized microarray expression values of ‘counter-regulated’ MHC class II genes are given for single microarray experiments, respectively for both 6-OHDA and vehicle injected rats. The mean slr of the HFS-effect equals the binary logarithm of

the fold change between the not stimulated and stimulated hemispheres of either 6-OHDA or vehicle injected rats. The mean slr of the lesion effect is calculated across groups between the non-stimulated hemispheres of vehicle and 6-OHDA injected rats. Counter-regulation is characterized by opposite regulation direction in the effect of lesion vs. the HFS-effect comparison. That is, STN-HFS normalizes expression values on the stimulated side of PD rats to values of controls on both stimulated and not stimulated hemispheres. RMA, robust multiarray averaging; 6-OHDA, 6-hydroxydopamine; slr, signal-log ratio; HFS, high-frequency stimulation; STN, subthalamic nucleus. (DOCX)

Acknowledgments

We thank Doris Lange for help with the histology, Kristin Klätschke for help with microarray experiments, Hauke Günther for help with RT-PCR analysis and Svenja Zapf for help with Western blot analysis.

Author Contributions

Conceived and designed the experiments: BG GE A. Sharott TS IP A. Schulte AKE CKEM WH. Performed the experiments: BG IP A. Schulte CKEM. Analyzed the data: BG A. Sharott TS IP A. Schulte CKEM. Contributed reagents/materials/analysis tools: TS IP A. Schulte MW KL AKE WH. Wrote the paper: BG A. Schulte CN IP CKEM WH.

References

- Albin RL, Young AB, Penney JB (1989) The functional anatomy of basal ganglia disorders. *Trends Neurosci* 12: 366–375.
- DeLong MR (1990) Primate models of movement disorders of basal ganglia origin. *Trends Neurosci* 13: 281–285.
- Benabid AL, Pollak P, Gross C, Hoffmann D, Benazzouz A, et al. (1994) Acute and long-term effects of subthalamic nucleus stimulation in Parkinson’s disease. *Stereotact Funct Neurosurg* 62: 76–84.
- Deuschl G, Schade-Brittinger C, Krack P, Volkmann J, Schäfer H, et al. (2006) A randomized trial of deep-brain stimulation for Parkinson’s disease. *N Engl J Med* 355: 896–908. doi:10.1056/NEJMoa060281.
- Krack P, Fraix V, Mendes A, Benabid AL, Pollak P (2002) Postoperative management of subthalamic nucleus stimulation for Parkinson’s disease. *Mov Disord* 17 Suppl 3: S188–97.
- Temperli P, Ghika J, Villemure JG, Burkhard PR, Bogousslavsky J, et al. (2003) How do parkinsonian signs return after discontinuation of subthalamic DBS? *Neurology* 60: 78–81.
- Shen KZ, Zhu ZT, Munhall A, Johnson SW (2003) Synaptic plasticity in rat subthalamic nucleus induced by high-frequency stimulation. *Synapse* 50: 314–319. doi:10.1002/syn.10274.
- Harnack D, Meissner W, Jira JA, Winter C, Morgenstern R, et al. (2008) Placebo-controlled chronic high-frequency stimulation of the subthalamic nucleus preserves dopaminergic nigral neurons in a rat model of progressive Parkinsonism. *Exp Neurol* 210: 257–260. doi:10.1016/j.expneurol.2007.10.002.
- Spiegel-Engemann AL, Steece-Collier K, Behbehani MM, Collier TJ, Wohlgenant SL, et al. (2011) Subthalamic Nucleus Stimulation Increases Brain Derived Neurotrophic Factor in the Nigrostriatal System and Primary Motor Cortex. *J Parkinsons Dis* 1: 123–136.
- Levy R, Hutchison WD, Lozano AM, Dostrovsky JO (2002) Synchronized neuronal discharge in the basal ganglia of parkinsonian patients is limited to oscillatory activity. *J Neurosci* 22: 2855–2861. doi:20026193.
- Bar-Gad I, Morris G, Bergman H (2003) Information processing, dimensionality reduction and reinforcement learning in the basal ganglia. *Prog Neurobiol* 71: 439–473. doi:10.1016/j.pneurobio.2003.12.001.
- Monakow KH, Akert K, Künzle H (1978) Projections of the precentral motor cortex and other cortical areas of the frontal lobe to the subthalamic nucleus in the monkey. *Exp Brain Res* 33: 395–403.
- Kitai ST, Deniau JM (1981) Cortical inputs to the subthalamus: intracellular analysis. *Brain Res* 214: 411–415.
- Nambu A (2005) A new approach to understand the pathophysiology of Parkinson’s disease. *J Neurol* 252 Suppl 4: IV1–IV4. doi:10.1007/s00415-005-4002-y.
- Li S, Arbutnot GW, Jutras MJ, Goldberg JA, Jaeger D (2007) Resonant antidromic cortical circuit activation as a consequence of high-frequency subthalamic deep-brain stimulation. *J Neurophysiol* 98: 3525–3537. doi:10.1152/jn.00808.2007.
- Gradinaru V, Mogri M, Thompson KR, Henderson JM, Deisseroth K (2009) Optical deconstruction of parkinsonian neural circuitry. *Science* 324: 354–359. doi:10.1126/science.1167093.
- Dejean C, Hyland B, Arbutnot G (2009) Cortical effects of subthalamic stimulation correlate with behavioral recovery from dopamine antagonist induced akinesia. *Cereb Cortex* 19: 1055–1063. doi:10.1093/cercor/bhn149.
- Ashby P, Paradiso G, Saint-Cyr JA, Chen R, Lang AE, et al. (2001) Potentials recorded at the scalp by stimulation near the human subthalamic nucleus. *Clin Neurophysiol* 112: 431–437.
- Baker KB, Montgomery EB Jr, Rezaei AR, Burgess R, Lüders HO (2002) Subthalamic nucleus deep brain stimulus evoked potentials: physiological and therapeutic implications. *Mov Disord* 17: 969–983. doi:10.1002/mds.10206.
- MacKinnon CD, Webb RM, Silberstein P, Tisch S, Asselman P, et al. (2005) Stimulation through electrodes implanted near the subthalamic nucleus activates projections to motor areas of cerebral cortex in patients with Parkinson’s disease. *Eur J Neurosci* 21: 1394–1402. doi:10.1111/j.1460-9568.2005.03952.x.
- Kuriakose R, Saha U, Castillo G, Udupa K, Ni Z, et al. (2010) The nature and time course of cortical activation following subthalamic stimulation in Parkinson’s disease. *Cereb Cortex* 20: 1926–1936. doi:10.1093/cercor/bhp269.
- Walker HC, Huang H, Gonzalez CL, Bryant JE, Killen J, et al. (2012) Short latency activation of cortex by clinically effective thalamic brain stimulation for tremor. *Mov Disord* 27: 1404–1412. doi:10.1002/mds.25137.
- Schulte T, Brecht S, Herdegen T, Illert M, Mehdorn HM, et al. (2006) Induction of immediate early gene expression by high-frequency stimulation of the subthalamic nucleus in rats. *Neuroscience* 138: 1377–1385. doi:10.1016/j.neuroscience.2005.12.034.
- Pennypacker KR, Hong JS, McMillan MK (1995) Implications of prolonged expression of Fos-related antigens. *Trends Pharmacol Sci* 16: 317–321.
- Kádár E, Lim LW, Carreras G, Genis D, Temel Y, et al. (2011) High-frequency stimulation of the ventrolateral thalamus regulates gene expression in hippocampus, motor cortex and caudate-putamen. *Brain Res* 1391: 1–13. doi:10.1016/j.brainres.2011.03.059.
- Henning J, Koczan D, Glass A, Karopka T, Pahnke J, et al. (2007) Deep brain stimulation in a rat model modulates TH, CaMKIIa and Homer1 gene expression. *Eur J Neurosci* 25: 239–250. doi:10.1111/j.1460-9568.2006.05264.x.
- Schwartz RK, Huston JP (1996) The unilateral 6-hydroxydopamine lesion model in behavioral brain research. Analysis of functional deficits, recovery and treatments. *Prog Neurobiol* 50: 275–331.
- Sakai K, Gash DM (1994) Effect of bilateral 6-OHDA lesions of the substantia nigra on locomotor activity in the rat. *Brain Res* 633: 144–150.
- Ferro MM, Bellissimo MI, Anselmo-Franci JA, Angellucci MEM, Canteras NS, et al. (2005) Comparison of bilaterally 6-OHDA- and MPTP-lesioned rats as models of the early phase of Parkinson’s disease: histological, neurochemical, motor and memory alterations. *J Neurosci Methods* 148: 78–87. doi:10.1016/j.jneumeth.2005.04.005.
- Paxinos G, Watson C (2005) *The Rat Brain in Stereotaxic Coordinates*. 5th ed. Sydney, Australia: Academic Press.
- Temel Y, Visser-Vandewalle V, Aendekerk B, Rutten B, Tan S, et al. (2005) Acute and separate modulation of motor and cognitive performance in

- parkinsonian rats by bilateral stimulation of the subthalamic nucleus. *Exp Neurol* 193: 43–52. doi:10.1016/j.expneurol.2004.12.025.
32. Gimsa U, Schreiber U, Habel B, Flehr J, van Rienen U, et al. (2006) Matching geometry and stimulation parameters of electrodes for deep brain stimulation experiments—numerical considerations. *J Neurosci Methods* 150: 212–227. doi:10.1016/j.jneumeth.2005.06.013.
 33. Grieb B, von Nicolai C, Engler G, Sharott A, Papageorgiou I, et al. (2013) Decomposition of abnormal free locomotor behavior in a rat model of Parkinson's disease. *Front Syst Neurosci* 7: 95. doi:10.3389/fnsys.2013.00095.
 34. Drai D, Benjamini Y, Golani I (2000) Statistical discrimination of natural modes of motion in rat exploratory behavior. *J Neurosci Methods* 96: 119–131.
 35. Harnack D, Winter C, Meissner W, Reum T, Kupsch A, et al. (2004) The effects of electrode material, charge density and stimulation duration on the safety of high-frequency stimulation of the subthalamic nucleus in rats. *J Neurosci Methods* 138: 207–216. doi:10.1016/j.jneumeth.2004.04.019.
 36. Darbaky Y, Forni C, Amalric M, Baunez C (2003) High frequency stimulation of the subthalamic nucleus has beneficial antiparkinsonian effects on motor functions in rats, but less efficiency in a choice reaction time task. *Eur J Neurosci* 18: 951–956.
 37. Liu F, Paule MG, Ali S, Wang C (2011) Ketamine-induced neurotoxicity and changes in gene expression in the developing rat brain. *Curr Neuropharmacol* 9: 256–261. doi:10.2174/157015911795017155.
 38. Kemmel V, Klein C, Dembélé D, Jost B, Taleb O, et al. (2010) A single acute pharmacological dose of γ -hydroxybutyrate modifies multiple gene expression patterns in rat hippocampus and frontal cortex. *Physiol Genomics* 41: 146–160. doi:10.1152/physiolgenomics.00208.2009.
 39. West MJ, Slomianka L, Gundersen HJ (1991) Unbiased stereological estimation of the total number of neurons in the subdivisions of the rat hippocampus using the optical fractionator. *Anat Rec* 231: 482–497. doi:10.1002/ar.1092310411.
 40. West MJ (2002) Design-based stereological methods for counting neurons. *Prog Brain Res* 135: 43–51. doi:10.1016/S0079-6123(02)35006-4.
 41. Gundersen HJ (1986) Stereology of arbitrary particles. A review of unbiased number and size estimators and the presentation of some new ones, in memory of William R. Thompson. *J Microsc* 143: 3–45.
 42. Gundersen HJ, Jensen EB (1987) The efficiency of systematic sampling in stereology and its prediction. *J Microsc* 147: 229–263.
 43. Temel Y, Visser-Vandewalle V, van der Wolf M, Spincemaille GH, Desbonnet L, et al. (2004) Monopolar versus bipolar high frequency stimulation in the rat subthalamic nucleus: differences in histological damage. *Neurosci Lett* 367: 92–96. doi:10.1016/j.neulet.2004.05.087.
 44. Agnew WF, Yuen TG, McCreery DB, Bullara LA (1986) Histopathologic evaluation of prolonged intracortical electrical stimulation. *Exp Neurol* 92: 162–185.
 45. Abd Alla J, Reeck K, Langer A, Streichert T, Quitterer U (2009) Calcitriol enhances B2 bradykinin receptor maturation and heterodimerization. *Biochem Biophys Res Commun* 387: 186–190. doi:10.1016/j.bbrc.2009.07.011.
 46. Panda S, Antoch MP, Miller BH, Su AL, Schook AB, et al. (2002) Coordinated transcription of key pathways in the mouse by the circadian clock. *Cell* 109: 307–320.
 47. Cirelli C, Gutierrez CM, Tononi G (2004) Extensive and divergent effects of sleep and wakefulness on brain gene expression. *Neuron* 41: 35–43.
 48. Dennis G Jr, Sherman BT, Hosack DA, Yang J, Gao W, et al. (2003) DAVID: Database for Annotation, Visualization, and Integrated Discovery. *Genome Biol* 4: P3.
 49. Huang DW, Sherman BT, Lempicki RA (2009) Systematic and integrative analysis of large gene lists using DAVID bioinformatics resources. *Nat Protoc* 4: 44–57. doi:10.1038/nprot.2008.211.
 50. Schulte A, Günther HS, Phillips HS, Kemming D, Martens T, et al. (2011) A distinct subset of glioma cell lines with stem cell-like properties reflects the transcriptional phenotype of glioblastomas and overexpresses CXCR4 as therapeutic target. *Glia* 59: 590–602. doi:10.1002/glia.21127.
 51. Hummon AB, Lim SR, Difilippantonio MJ, Ried T (2007) Isolation and solubilization of proteins after TRIzol extraction of RNA and DNA from patient material following prolonged storage. *BioTechniques* 42: 467–470, 472.
 52. Fox CM, Gash DM, Smoot MK, Cass WA (2001) Neuroprotective effects of GDNF against 6-OHDA in young and aged rats. *Brain Res* 896: 56–63.
 53. Strackx E, Van den Hove DLA, Steinbusch HP, Steinbusch HWM, Vles JSH, et al. (2008) A combined behavioral and morphological study on the effects of fetal asphyxia on the nigrostriatal dopaminergic system in adult rats. *Exp Neurol* 211: 413–422. doi:10.1016/j.expneurol.2008.02.006.
 54. Healy-Stoffel M, Ahmad SO, Stanford JA, Levant B (2012) A novel use of combined tyrosine hydroxylase and silver nucleolar staining to determine the effects of a unilateral intrastriatal 6-hydroxydopamine lesion in the substantia nigra: a stereological study. *J Neurosci Methods* 210: 187–194. doi:10.1016/j.jneumeth.2012.07.013.
 55. Walker QD, Johnson ML, Van Swearingen AED, Arrant AE, Caster JM, et al. (2012) Individual differences in psychostimulant responses of female rats are associated with ovarian hormones and dopamine neuroanatomy. *Neuropharmacology* 62: 2267–2277. doi:10.1016/j.neuropharm.2012.01.029.
 56. Zaidel A, Spivak A, Grieb B, Bergman H, Israel Z (2010) Subthalamic span of beta oscillations predicts deep brain stimulation efficacy for patients with Parkinson's disease. *Brain* 133: 2007–2021. doi:10.1093/brain/awq144.
 57. Chung SJ, Jeon SR, Kim SR, Sung YH, Lee MC (2006) Bilateral effects of unilateral subthalamic nucleus deep brain stimulation in advanced Parkinson's disease. *Eur Neurol* 56: 127–132. doi:10.1159/000095704.
 58. Alberts JL, Hass CJ, Vitek JL, Okun MS (2008) Are two leads always better than one: an emerging case for unilateral subthalamic deep brain stimulation in Parkinson's disease. *Exp Neurol* 214: 1–5. doi:10.1016/j.expneurol.2008.07.019.
 59. Walker HC, Watts RL, Guthrie S, Wang D, Guthrie BL (2009) Bilateral effects of unilateral subthalamic deep brain stimulation on Parkinson's disease at 1 year. *Neurosurgery* 65: 302–9; discussion 309–10. doi:10.1227/01.NEU.0000349764.34211.74.
 60. Tan S, Rudd JA, Yew DT (2011) Gene Expression Changes in GABA_A Receptors and Cognition Following Chronic Ketamine Administration in Mice. *PLoS ONE* 6: e21328. doi:10.1371/journal.pone.0021328.
 61. Raz A, Eimerl D, Zaidel A, Bergman H, Israel Z (2010) Propofol decreases neuronal population spiking activity in the subthalamic nucleus of Parkinsonian patients. *Anesth Analg* 111: 1285–1289. doi:10.1213/ANE.0b013e3181f56f2.
 62. Hirsch E, Graybiel AM, Agid YA (1988) Melanized dopaminergic neurons are differentially susceptible to degeneration in Parkinson's disease. *Nature* 334: 345–348. doi:10.1038/334345a0.
 63. Uhl GR, Hedreen JC, Price DL (1985) Parkinson's disease: loss of neurons from the ventral tegmental area contralateral to therapeutic surgical lesions. *Neurology* 35: 1215–1218.
 64. Dymecki J, Lechowicz W, Bertrand E, Szpak GM (1996) Changes in dopaminergic neurons of the mesocorticolimbic system in Parkinson's disease. *Folia Neuropathol* 34: 102–106.
 65. McRitchie DA, Cartwright HR, Halliday GM (1997) Specific A10 dopaminergic nuclei in the midbrain degenerate in Parkinson's disease. *Exp Neurol* 144: 202–213. doi:10.1006/exnr.1997.6418.
 66. Thobois S, Ardouin C, Lhommée E, Klinger H, Lagrange C, et al. (2010) Non-motor dopamine withdrawal syndrome after surgery for Parkinson's disease: predictors and underlying mesolimbic denervation. *Brain* 133: 1111–1127. doi:10.1093/brain/awq032.
 67. Hammond C, Bergman H, Brown P (2007) Pathological synchronization in Parkinson's disease: networks, models and treatments. *Trends Neurosci* 30: 357–364. doi:10.1016/j.tins.2007.05.004.
 68. Sharott A, Magill PJ, Harnack D, Kupsch A, Meissner W, et al. (2005) Dopamine depletion increases the power and coherence of beta-oscillations in the cerebral cortex and subthalamic nucleus of the awake rat. *Eur J Neurosci* 21: 1413–1422. doi:10.1111/j.1460-9568.2005.03973.x.
 69. Brazhnik E, Cruz AV, Avila I, Wahba MI, Novikov N, et al. (2012) State-Dependent Spike and Local Field Synchronization between Motor Cortex and Substantia Nigra in Hemiparkinsonian Rats. *J Neurosci* 32: 7869–7880. doi:10.1523/JNEUROSCI.0943-12.2012.
 70. Cassidy M, Mazzone P, Oliviero A, Insola A, Tonali P, et al. (2002) Movement-related changes in synchronization in the human basal ganglia. *Brain* 125: 1235–1246.
 71. Vogel C, Marcotte EM (2012) Insights into the regulation of protein abundance from proteomic and transcriptomic analyses. *Nat Rev Genet* 13: 227–232. doi:10.1038/nrg3185.
 72. Tian Q, Stepanians SB, Mao M, Weng L, Feetham MC, et al. (2004) Integrated genomic and proteomic analyses of gene expression in Mammalian cells. *Mol Cell Proteomics* 3: 960–969. doi:10.1074/mcp.M400055-MCP200.
 73. Schwahnhauser B, Busse D, Li N, Dittmar G, Schuchhardt J, et al. (2011) Global quantification of mammalian gene expression control. *Nature* 473: 337–342. doi:10.1038/nature10098.
 74. Sarro SM, Unruh TL, Zuccolo J, Sanyal R, Luidner JM, et al. (2010) Quantification of CD20 mRNA and protein levels in chronic lymphocytic leukemia suggests a post-transcriptional defect. *Leuk Res* 34: 1670–1673. doi:10.1016/j.leukres.2010.06.031.
 75. Shebl FM, Pinto LA, García-Piñeres A, Lempicki R, Williams M, et al. (2010) Comparison of mRNA and protein measures of cytokines following vaccination with human papillomavirus-16 L1 virus-like particles. *Cancer Epidemiol Biomarkers Prev* 19: 978–981. doi:10.1158/1055-9965.EPI-10-0064.
 76. Wong GH, Bartlett PF, Clark-Lewis I, Battye F, Schrader JW (1984) Inducible expression of H-2 and Ia antigens on brain cells. *Nature* 310: 688–691.
 77. McGeer PL, Itagaki S, Boyes BE, McGeer EG (1988) Reactive microglia are positive for HLA-DR in the substantia nigra of Parkinson's and Alzheimer's disease brains. *Neurology* 38: 1285–1291.
 78. Akiyama H, McGeer PL (1989) Microglial response to 6-hydroxydopamine-induced substantia nigra lesions. *Brain Res* 489: 247–253.
 79. Imamura K, Hishikawa N, Sawada M, Nagatsu T, Yoshida M, et al. (2003) Distribution of major histocompatibility complex class II-positive microglia and cytokine profile of Parkinson's disease brains. *Acta Neuropathol* 106: 518–526. doi:10.1007/s00401-003-0766-2.
 80. Hävik B, Rokke H, Dagey G, Stavrum AK, Bramham CR, et al. (2007) Synaptic activity-induced global gene expression patterns in the dentate gyrus of adult behaving rats: induction of immunity-linked genes. *Neuroscience* 148: 925–936. doi:10.1016/j.neuroscience.2007.07.024.
 81. Corriveau RA, Huh GS, Shatz CJ (1998) Regulation of class I MHC gene expression in the developing and mature CNS by neural activity. *Neuron* 21: 505–520.

82. Huh GS, Boulanger LM, Du H, Riquelme PA, Brotz TM, et al. (2000) Functional requirement for class I MHC in CNS development and plasticity. *Science* 290: 2155–2159.
83. Neumann H, Boucraut J, Hahnel C, Misgeld T, Wekerle H (1996) Neuronal control of MHC class II inducibility in rat astrocytes and microglia. *Eur J Neurosci* 8: 2582–2590.
84. Neumann H, Misgeld T, Matsumuro K, Wekerle H (1998) Neurotrophins inhibit major histocompatibility class II inducibility of microglia: involvement of the p75 neurotrophin receptor. *Proc Natl Acad Sci U S A* 95: 5779–5784.
85. Neumann H (2001) Control of glial immune function by neurons. *Glia* 36: 191–199.

Supporting information

Gene symbol	Affymetrix ID	6-OHDA: STN-HFS-effect					Vehicle: STN-HFS-effect					Lesion-effect
		slr	signal stim		signal no-stim		slr	signal stim		signal no-stim		
		mean	MA1	MA2	MA1	MA2	mean	MA1	MA2	MA1	MA2	
RT1-Db1	1370383_s_at	-2.7	49.7	318.5	1004.4	623.3	-	173.9	363	199.7	272.4	1.9
RT1-Da	1370883_at	-2.7	193.3	1157.9	4215.7	2001.5	-	721.5	1072.8	1007.1	915.3	1.5
RT1-Bb	1371033_at	-2.6	52.9	266.5	938.4	627.8	-	159.9	305.3	260	255.9	1.5
Cd74	1367679_at	-2.4	402	2180.5	6785.3	3795.2	-	1769.4	2225.8	2479.7	1765.6	1.2
RT1-Ba	1381593_x_at	-2.4	315.1	1824.3	4493	3368.4	-	1339.3	2039.5	1874.4	1792.9	1.2

Table 1: Microarray expression values MHC class II genes. RMA-normalized microarray expression values of ‘counter-regulated’ MHC class II genes are given for single microarray experiments, respectively for both 6-OHDA and vehicle injected rats. The mean slr of the HFS-effect equals the binary logarithm of the fold change between the not stimulated and stimulated hemispheres of either 6-OHDA or vehicle injected rats. The mean slr of the lesion effect is calculated across groups between the non-stimulated hemispheres of vehicle and 6-OHDA injected rats. Counter-regulation is characterized by opposite regulation direction in the effect of lesion vs. the HFS-effect comparison. That is, STN-HFS normalizes expression values on the stimulated side of PD rats to values of controls on both stimulated and not stimulated hemispheres. (Abbreviations: RMA, robust multiarray averaging; 6-OHDA, 6-hydroxydopamine; slr, signal-log ratio; HFS, high-frequency stimulation; STN, subthalamic nucleus)

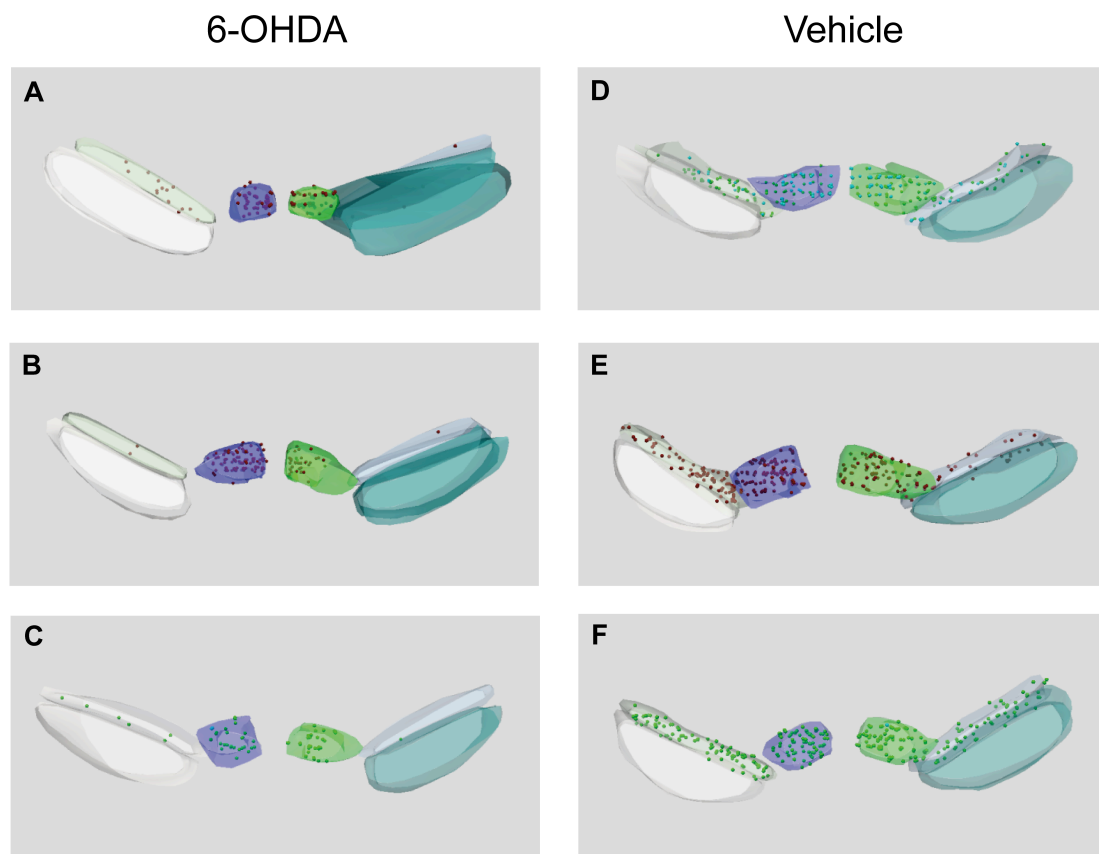


Figure 1: 3-D reconstructions of stereology. Panels (A-F) depict 3D-reconstructions of stereological regions of interest for all 6-OHDA (left column) or vehicle injected rats (right column) used in gene expression profiling. Different ROIs are color-coded (white: left SNr, pale green: left SNc, purple: left VTA, green: right VTA, pale blue: right SNc, cyan: right SNr). Stereological cell counting was only performed in VTA and SNc-ROIs. Spheres indicate stereologically counted cells in the SNc and VTA. (Abbreviations: 6-OHDA, 6-hydroxydopamine; ROI, region of interest; SNr, substantia nigra pars reticulata; SNc, substantia nigra pars compacta; VTA, ventral tegmental area)

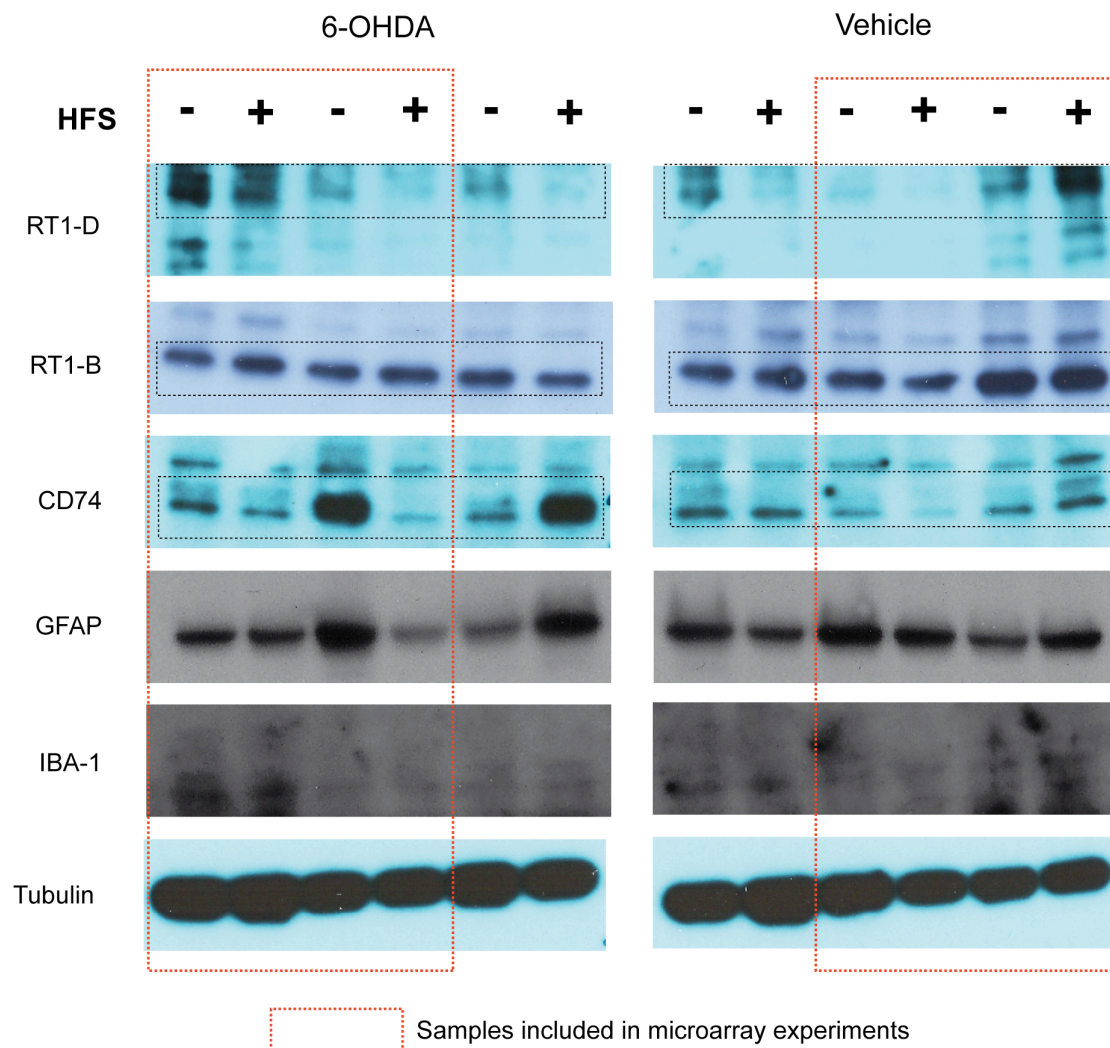


Figure 2: Western blot analysis. Detection of MHC class II candidate proteins (RT1-D, RT1-B, CD74), astroglial (GFAP) and microglial (Iba-1) markers by Western blot analysis. All candidates belonged to the enriched gene cluster ‘antigen processing and presentation of peptide antigen.’ The housekeeping protein tubulin served as biological control. All twelve lanes for a given antigen were blotted simultaneously and cropped later for graphical display. (Abbreviations: 6-OHDA, 6-hydroxydopamine; HFS, high-frequency stimulation; MHC, major histocompatibility complex)

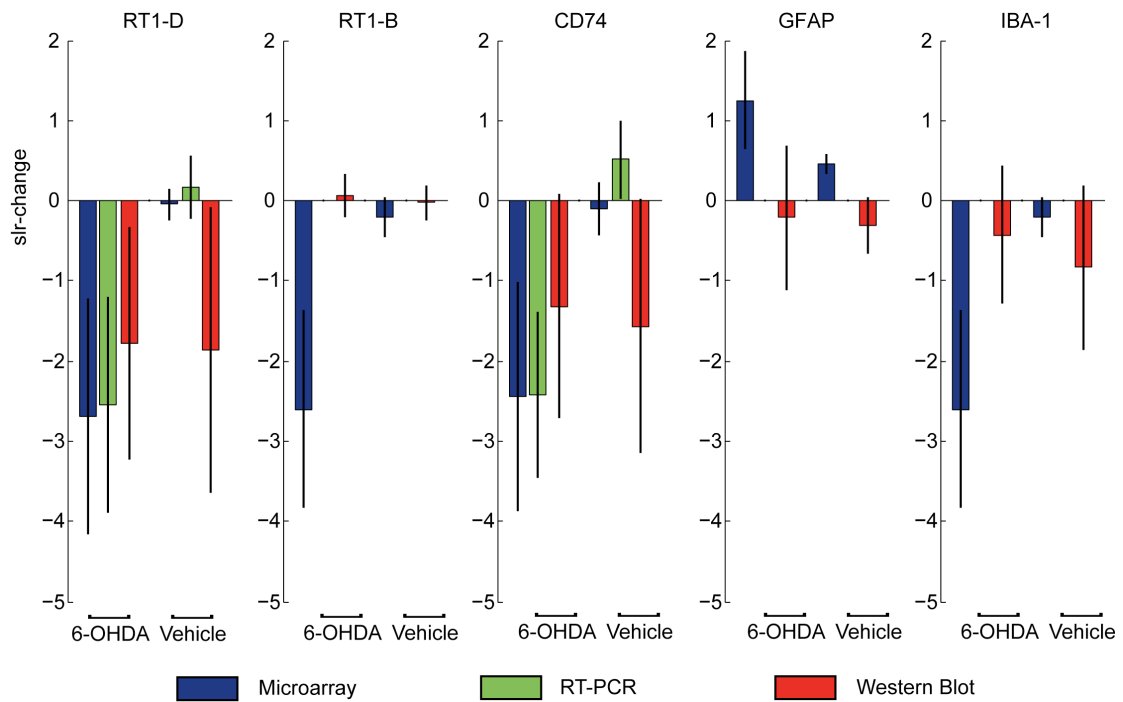


Figure 3: Comparison of microarray, RT-PCR and Western blot regulation changes. Quantification of signal-log ratio (slr) changes of MHC class II candidates (RT1-D, RT1-B, CD74), astroglial (GFAP) and microglial (Iba-1) markers. We utilized densitometric quantification to evaluate protein levels in Western blots. No statistical comparison was applied due to low sample size and missing data regarding RT-PCR (RT1-B, GFAP and Iba-1 were only investigated by Western blotting).

Summary

Summary

Parkinson's disease (PD) is a chronic, progressive neurodegenerative disorder first described by James Parkinson in 1817 (Parkinson, 1817). About 1% of the population over 60 years of age are suffering from this disease making it the second most frequent neurodegenerative disorder after Alzheimer's disease (de Lau & Breteler, 2006). Its core symptoms are resting tremor, rigor and akinesia (Jankovic, 2008).

The pathological hallmark of PD is the degeneration of neurons in the substantia nigra pars compacta (SNc), which leads to degeneration of the nigrostriatal pathway (Obeso, Rodriguez-Oroz, Rodriguez, *et al.*, 2000). However, the exact mechanisms of the chronic and progressive neurodegeneration in PD still remain elusive. Motor symptoms only tend to occur after the degree of striatal dopamine depletion exceeds approximately 80% (Bernheimer, Birkmayer, Hornykiewicz, *et al.*, 1973). The histopathological finding of filamentous, cytoplasmatic inclusions termed Lewy bodies in surviving dopaminergic neurons of the SNc, but also in the cortex or the magnocellular basal forebrain nuclei, represents a pathological diagnostic marker of PD (Gibb & Lees, 1988). Lewy bodies are invariably present in all diagnosed cases of PD and contain the protein alpha-synuclein (Spillantini, Schmidt, Lee, *et al.*, 1997). Lewy bodies tend to occur in sites of excessive neuronal cell loss and the formation of altered neurofilament may result from a cell's incapability to fully process cellular debris caused by excessive oxidative stress and mitochondrial dysfunction (Halliwell, 1992; Cassarino, Fall, Swerdlow, *et al.*, 1997).

Important pathophysiological changes in the basal ganglia-thalamo-cortical circuit, which ultimately lead to the behavioral features of PD, are characterized by synchronized neuronal activity. Such oscillatory activity within the beta (13-30 Hz) frequency band can be recorded in basal ganglia nuclei, thalamus and frontal cortex in human PD patients (Brown, Oliviero,

Mazzone, *et al.*, 2001; Brown, 2003; Engel, Moll, Fried, *et al.*, 2005) as well as in animal models of PD (Sharott, Magill, Harnack, *et al.*, 2005; Mallet, Pogosyan, Sharott, *et al.*, 2008). Dopamine administration and voluntary movement reduce the magnitude of pathological oscillatory activity (Levy, Ashby, Hutchison, *et al.*, 2002), which in essence seems to inhibit movement (Brown, 2006; Engel & Fries, 2010).

Summary of Part A

The first agent with a specific neurotoxic effect on catecholaminergic neurons discovered was 6-hydroxydopamine (6-OHDA; Porter, Totaro & Stone, 1963; Ungerstedt, 1968). Its cellular toxicity is derived from an excessive production of hydrogen peroxide, hydroxyl radicals and superoxide free radicals in the presence of iron. As 6-OHDA is not able to cross the blood-brain barrier it has to be administered locally in experimental animals by intracranial infusion. Typical targets of stereotaxic surgery are the SNc and the striatum, the medial forebrain bundle connecting both structures, and the lateral ventricle. If administered into one of these structures, 6-OHDA causes an acute degeneration of the nigrostriatal pathway within 1-3 days. Most often 6-OHDA is injected into one hemisphere only, creating a hemi-parkinsonian animal model (Schwartzing & Huston, 1996a, 1996b). In this case, motor symptoms are relatively mild and appear, e.g., as limb use asymmetry (Tillerson, Cohen, Philhower, *et al.*, 2001) or gait disturbance (Metz, Tse, Ballermann, *et al.*, 2005). If 6-OHDA is injected bilaterally the resulting movement deficits are more pronounced, rendering the animal severely hypo- and bradykinetic (Schallert, Whishaw, Ramirez, *et al.*, 1978; Sakai & Gash, 1994). Tremor is not caused regularly. Due to coinciding bilateral depletion of the mesolimbic dopaminergic system, also non-motor symptoms like aphagia, adipsia and abulia can appear (Sakai & Gash, 1994; Ferro, Bellissimo, Anselmo-Franci, *et al.*, 2005), causing difficulties in

sustaining the animals during long-term behavioral experiments. For this reason, the bilateral 6-OHDA rat model has not been intensively studied in the past, although it mimics the behavioral symptoms of PD, especially akinesia, more closely than the unilateral model.

Part A of this thesis addresses the movement deficits of bilaterally lesioned 6-OHDA rats. To analyze the fine structure of motor symptoms we employed analysis techniques first described by Draï et al. (Draï, Benjamini & Golani, 2000; Draï & Golani, 2001) on video-tracking data obtained from 23 hours of locomotion monitoring. The analysis is based on measuring the maximal movement speed accomplished within a single given motion episode. As a comparison, if all single motion episodes of one recording session would make up a full mountain range, the unfolding panoramic view would be characterized by the maximal altitude rather than the average height of its peaks. The distribution of peaks can therefore reveal a speed profile with distinct modes of motions, which Draï et al. termed “gears”.

In this study, bilaterally lesioned 6-OHDA rats exhibited a selective decrease of faster “second gear” episodes. That is, the distribution of maximal speeds revealed an obvious correlate of bradykinesia, while also the total number of motion episodes was diminished indicating a more general poverty of movement or akinesia. The isolation of separate motion episodes also allowed quantification of the spatial spread and dwell time of single episodes. Unexpectedly, both parameters were enlarged in PD rats. This finding could relate to kinesia paradoxa, describing unexpected bouts of locomotion in otherwise severely akinetic PD patients (Martin, 1967). Due to a sampling rate of ~13Hz of the recording the tracking data revealed the naturalistic shape of the rat’s walking path. Analyzing the curvature of these traces revealed an increased curvature index for 6-OHDA treated rats, which could relate to abnormal hind limb rigidity, present in manual inspection. Interestingly, the facilitation of faster movement episodes resulted in straighter movement traces, also in PD rats.

In conclusion, Part A of this thesis represents the first report of detailed locomotion analysis of spontaneous and long-term movement observations of bilaterally lesioned parkinsonian rats. The applied behavioral analysis could be extended by in-vivo electrophysiology to investigate the neuronal mechanisms underlying abnormal locomotion due to dopamine depletion. Furthermore, it enables behavioral phenotyping of single rats, which can be useful for later experiments that rely on the individual disease state.

Summary of Part B

A widely established treatment option of medically refractory PD is the chronic application of high-frequency stimulation (also termed “deep brain stimulation”) to areas along the basal ganglia-thalamo-cortical loop. Nowadays, the most often targeted structure for implantation of stimulation leads is the subthalamic nucleus (STN; Benabid, Pollak, Gross, *et al.*, 1994; Deuschl, Schade-Brittinger, Krack, *et al.*, 2006). Within the classical framework of basal ganglia pathophysiology, STN-HFS is thought to reduce excessive activity of the “indirect pathway”, comparable to the non-reversible surgical lesion of the STN (Bergman, Wichmann & DeLong, 1990), leading to alleviation of PD symptoms. Other studies emphasize retrograde activation of the “hyperdirect pathway”, in which cortical projections form a monosynaptic connection with the STN (Nambu, 2005). In both cases, pathophysiological changes in the sensorimotor cortex, as in the basal ganglia, are involved in generating parkinsonian motor symptoms. Interestingly, the alleviation of motor symptoms by STN-HFS happens with a temporal delay for certain symptoms, as does the reoccurrence of symptoms after switching of the stimulation (Temperli, Ghika, Villemure, *et al.*, 2003). Immediate alteration of neuronal activity due to HFS can hardly explain such a delay and calls for the involvement of plastic changes on a longer time scale. Regarding such changes, mRNA transcription represents the

most upstream step and basically the main switch for operating the more or less fixed genetic code. Although proteins bring about phenotypic changes and convey cellular functions, the detection of induced or repressed genes stands for a shift in the currently activated genetic program at the most fundamental level.

In Part B of this thesis, gene expression changes of sensorimotor cortical tissue following longer-term STN-HFS in parkinsonian rats were explored using Affymetrix®-microarray gene chip technology. Gene chips enable screening investigations of the complete transcriptome to either identify induced or repressed single target genes or entire gene networks in comparison to a control. A major advantage in using bilaterally 6-OHDA lesioned rats is the ability of stimulating only one hemisphere and using the non-stimulated hemisphere as control, thereby using the same animal as its own experimental control regarding gene expression profiling. Thus, biological variability between animals would not influence the identification of regulated genes possibly relevant for STN-HFS in a single parkinsonian rat. The profiling within PD rats could be further compared to profiling in sham treated controls to elucidate the specific effects of STN-HFS in a diseased system. To guarantee high similarity between single experimental animals all rats were monitored behaviorally to quantify apparent brady- and akinesia (see also Part A). The stereotactic coordinates for placing stimulation leads within the STN were adapted after electrophysiological delineation of the STN boundaries by assessing typical STN multi-unit activity. Furthermore, recordings of local field potentials from the frontal cortex and the STN in the awake animal revealed excessive oscillatory activity within the high-beta/low-gamma frequency range. That is, bilaterally lesioned rats exhibited slightly higher frequencies of pathological oscillations as compared to unilaterally lesioned 6-OHDA rats (Sharott, Magill, Harnack, *et al.*, 2005; Mallet, Pogosyan, Sharott, *et al.*, 2008). However, generating

bilaterally lesioned and chronically bilaterally implanted rats for long-term stimulation proved difficult, resulting in a small final number of animals used for gene expression experiments (N=3 for PD and N=3 for control rats). The obtained genetic data was hence analyzed with a conservative approach utilizing both within and across animal comparisons. Candidate genes were investigated by RT-PCR analyses and downstream protein abundance by Western Blotting.

The only genes that showed significant regulation in all analysis steps were major histocompatibility complex (MHC) genes. Most involved MHC class II genes (RT1 class II, locus Da, locus Db1, locus Bb, locus Ba and CD74 antigen) and only one MHC class I gene (RT1 class I, CE5). All were strongly downregulated by STN-HFS only in PD rats. Interestingly, the same set of MHC class II genes showed upregulation in a comparison between the non-stimulated hemispheres of PD and control rats, which addressed the effect of 6-OHDA lesioning. Thus, MHC class II genes showed counter regulation by STN-HFS. This regulation pattern could derive from enhanced cortical microglial activity in the PD state and repressed cortical microglial activity by STN-DBS. However, western blot investigation of the microglial marker Iba-1 and the astroglial marker GFAP did not provide clear indication of altered microglial/astroglial activation.

In conclusion, Part B of this thesis describes the novel finding of cortical MHC class II gene downregulation in response to STN-HFS. Whether this regulation is due to altered glial or neuronal activity is not clear at the moment. Understanding the genetic and proteomic changes within the motor cortex in response to STN-HFS, which eventually lead to altered neuronal function of the cortical machinery, remains an exciting question for future research.

References

- Benabid, A.L., Pollak, P., Gross, C., Hoffmann, D., et al. (1994) Acute and long-term effects of subthalamic nucleus stimulation in Parkinson's disease. *Stereotact Funct Neurosurg.* 62 (1-4), 76–84.
- Bergman, H., Wichmann, T. & DeLong, M.R. (1990) Reversal of experimental parkinsonism by lesions of the subthalamic nucleus. *Science.* 249 (4975), 1436–1438.
- Bernheimer, H., Birkmayer, W., Hornykiewicz, O., Jellinger, K., et al. (1973) Brain dopamine and the syndromes of Parkinson and Huntington Clinical, morphological and neurochemical correlations. *Journal of the Neurological Sciences.* 20 (4), 415–455.
- Brown, P. (2006) Bad oscillations in Parkinson's disease. *J Neural Transm Suppl.* (70), 27–30.
- Brown, P. (2003) Oscillatory nature of human basal ganglia activity: relationship to the pathophysiology of Parkinson's disease. *Mov Disord.* 18 (4), 357–363.
- Brown, P., Oliviero, A., Mazzone, P., Insola, A., et al. (2001) Dopamine dependency of oscillations between subthalamic nucleus and pallidum in Parkinson's disease. *J Neurosci.* 21 (3), 1033–1038.
- Cassarino, D.S., Fall, C.P., Swerdlow, R.H., Smith, T.S., et al. (1997) Elevated reactive oxygen species and antioxidant enzyme activities in animal and cellular models of Parkinson's disease. *Biochimica et Biophysica Acta (BBA) - Molecular Basis of Disease.* 1362 (1), 77–86.
- Deuschl, G., Schade-Brittinger, C., Krack, P., Volkmann, J., et al. (2006) A randomized trial of deep-brain stimulation for Parkinson's disease. *N Engl J Med.* 355 (9), 896–908.
- Drai, D., Benjamini, Y. & Golani, I. (2000) Statistical discrimination of natural modes of motion in rat exploratory behavior. *J Neurosci Methods.* 96 (2), 119–131.
- Drai, D. & Golani, I. (2001) SEE: a tool for the visualization and analysis of rodent exploratory behavior. *Neurosci Biobehav Rev.* 25 (5), 409–426.
- Engel, A.K. & Fries, P. (2010) Beta-band oscillations—signalling the status quo? *Curr Opin Neurobiol.* 20 (2), 156–165.
- Engel, A.K., Moll, C.K.E., Fried, I. & Ojemann, G.A. (2005) Invasive recordings from the human brain: clinical insights and beyond. *Nature Reviews Neuroscience.* 6 (1), 35–47.
- Ferro, M.M., Bellissimo, M.I., Anselmo-Franci, J.A., Angellucci, M.E.M., et al. (2005) Comparison of bilaterally 6-OHDA- and MPTP-lesioned rats as models of the early phase of Parkinson's disease: histological, neurochemical, motor and memory alterations. *Journal of neuroscience methods.* 148 (1), 78–87.

- Gibb, W.R. & Lees, A.J. (1988) The relevance of the Lewy body to the pathogenesis of idiopathic Parkinson's disease. *Journal of Neurology, Neurosurgery & Psychiatry*. 51 (6), 745–752.
- Halliwell, B. (1992) Reactive Oxygen Species and the Central Nervous System. In: Lester Packer, Leonid Prilipko, & Yves Christen (eds.). *Free Radicals in the Brain*. [Online]. Springer Berlin Heidelberg. pp. 21–40.
- Jankovic, J. (2008) Parkinson's disease: clinical features and diagnosis. *Journal of Neurology, Neurosurgery & Psychiatry*. 79 (4), 368–376.
- De Lau, L.M.L. & Breteler, M.M.B. (2006) Epidemiology of Parkinson's disease. *Lancet Neurology*. 5 (6), 525–535.
- Levy, R., Ashby, P., Hutchison, W.D., Lang, A.E., et al. (2002) Dependence of subthalamic nucleus oscillations on movement and dopamine in Parkinson's disease. *Brain*. 125 (Pt 6), 1196–1209.
- Mallet, N., Pogosyan, A., Sharott, A., Csicsvari, J., et al. (2008) Disrupted dopamine transmission and the emergence of exaggerated beta oscillations in subthalamic nucleus and cerebral cortex. *J Neurosci*. 28 (18), 4795–4806.
- Martin, J. (1967) *The basal ganglia and posture*. Lippincott.
- Metz, G.A., Tse, A., Ballermann, M., Smith, L.K., et al. (2005) The unilateral 6-OHDA rat model of Parkinson's disease revisited: an electromyographic and behavioural analysis. *The European journal of neuroscience*. 22 (3), 735–744.
- Nambu, A. (2005) A new approach to understand the pathophysiology of Parkinson's disease. *J Neurol*. 252 Suppl 4IV1–IV4.
- Obeso, J.A., Rodriguez-Oroz, M.C., Rodriguez, M., Lanciego, J.L., et al. (2000) Pathophysiology of the basal ganglia in Parkinson's disease. *Trends in Neurosciences*. 23S8–S19.
- Parkinson, J. (1817) *An essay on the shaking palsy*. Whittingham and Rowland.
- Porter, C.C., Totaro, J.A. & Stone, C.A. (1963) Effect of 6-Hydroxydopamine and Some Other Compounds on the Concentration of Norepinephrine in the Hearts of Mice. *Journal of Pharmacology and Experimental Therapeutics*. 140 (3), 308–316.
- Sakai, K. & Gash, D.M. (1994) Effect of bilateral 6-OHDA lesions of the substantia nigra on locomotor activity in the rat. *Brain Res*. 633 (1-2), 144–150.
- Schallert, T., Wishaw, I.Q., Ramirez, V.D. & Teitelbaum, P. (1978) Compulsive, abnormal walking caused by anticholinergics in akinetic, 6-hydroxydopamine-treated rats. *Science (New York, N.Y.)*. 199 (4336), 1461–1463.

- Schwartz, R.K. & Huston, J.P. (1996a) The unilateral 6-hydroxydopamine lesion model in behavioral brain research. Analysis of functional deficits, recovery and treatments. *Prog Neurobiol.* 50 (2-3), 275–331.
- Schwartz, R.K. & Huston, J.P. (1996b) Unilateral 6-hydroxydopamine lesions of mesostriatal dopamine neurons and their physiological sequelae. *Prog Neurobiol.* 49 (3), 215–266.
- Sharott, A., Magill, P.J., Harnack, D., Kupsch, A., et al. (2005) Dopamine depletion increases the power and coherence of beta-oscillations in the cerebral cortex and subthalamic nucleus of the awake rat. *Eur J Neurosci.* 21 (5), 1413–1422.
- Spillantini, M.G., Schmidt, M.L., Lee, V.M.-Y., Trojanowski, J.Q., et al. (1997) α -Synuclein in Lewy bodies. *Nature.* 388 (6645), 839–840.
- Temperli, P., Ghika, J., Villemure, J.-G., Burkhard, P.R., et al. (2003) How do parkinsonian signs return after discontinuation of subthalamic DBS? *Neurology.* 60 (1), 78–81.
- Tillerson, J.L., Cohen, A.D., Philhower, J., Miller, G.W., et al. (2001) Forced Limb-Use Effects on the Behavioral and Neurochemical Effects of 6-Hydroxydopamine. *The Journal of Neuroscience.* 21 (12), 4427–4435.
- Ungerstedt, U. (1968) 6-hydroxy-dopamine induced degeneration of central monoamine neurons. *European Journal of Pharmacology.* 5 (1), 107–110.

Appendices

Danksagungen

An der Entstehung dieser Arbeit hatten viele Menschen Anteil. Ganz herzlich möchte ich an dieser Stelle danken: Meinen Eltern, Ulrike und Michael Grieb – für ihre bedingungslose Unterstützung und Liebe. Meinem Doktorvater, PD Dr. Wolfgang Hamel – für die Idee zu dieser Arbeit und die große Freundlichkeit, mit welcher er ihre Umsetzung begleitete. Meinem Betreuer, Christian K. Moll – für seine Beseelung der Basal Ganglien. Dr. Gerhard Engler – für seinen unbeugsamen Optimismus (und für die Virtuosität am LötKolben). Prof. Dr. Andreas K. Engel – für den stimulierenden Nährboden, in wissenschaftlicher und darüber hinaus gehender Hinsicht. Dr. Andy Sharott – for invaluable constructive criticism. Dr. Gernot (GG) Supp – für Inspiration, Bekanntmachung mit Kernöl und ein infektiöses Lachen. Dr. Ismini Papageorgiou – für das Licht der Stereologie. Dr. Alexander Schulte – für seinen Schwimmunterricht im Nasslabor. Dr. Thomas Streichert – für hilfreiche Wegweiser im Wald voller Bäume (Gene-Chip Technologie). Prof. Dr. Katrin Lamzus und Prof. Dr. Manfred Westphal – für wertvolle Hilfe und Beratung. Kristine Klätschke, Doris Lange und Svenja Zapf – für eine erstklassige technische Unterstützung. Prof. Dr. Sabine Herpertz, PD Dr. Knut Schnell und Prof. Dr. Thomas Kuner – für ihre unterstützende Haltung gegenüber der Fertigstellung dieser Arbeit. Meinem Wegbegleiter, Dr. Constantin von Nicolai – für eine Doktorarbeiten überdauernde Freundschaft. Meiner Ehefrau, Orit Nakar – für die Konzentration auf das Wesentliche.

Curriculum vitae

Personal information

Full name	Benjamin Max Grieb
Address	Franz Schubert Str. 8, 88213 Ravensburg
E-Mail	grieb.bm@gmail.com
Marital status	Married to Orit Nakar
Nationality	German
Date / place of birth	5. February 1982 in Mainz, Germany

Education

Since 2016	Training in psychiatry and psychotherapy , Center for Psychiatry South-Wuerttemberg, Ulm University, Department of Psychiatry I, Ravensburg
2014-2015	Training in neurology , Oberschwabenklinik Ravensburg, Department of Neurology
2011-2014	Training in cognitive behavioral psychotherapy , Center for Psychological Psychotherapy Heidelberg, University of Heidelberg
2011-2014	Training in psychiatry , Department of General Psychiatry, University of Heidelberg
Since 2009	License to practice medicine , City of Hamburg
2002- 2009	Medical studies , University Medical Center Hamburg-Eppendorf, University of Hamburg
2001	Abitur , Hansa-Gymnasium Bergedorf, Hamburg

Working experience

Since 2016	Assistant physician in psychiatry , Center for Psychiatry South-Wuerttemberg, Ulm University, Department of Psychiatry I, Ravensburg
2014-2015	Assistant physician in neurology , Oberschwabenklinik Ravensburg, Department of Neurology
2011-2014	Assistant physician in psychiatry , Department of General Psychiatry, University of Heidelberg
2011- 2014	Research fellowship , Institute for Anatomy and Cell Biology, University of Heidelberg
2009- 2011	Research fellowship , Department of Neurophysiology and Pathophysiology, University of Hamburg

- Grieb B, Engler G, Sharott A, von Nicolai C, Streichert T, et al. (2014) High-frequency stimulation of the subthalamic nucleus counteracts cortical expression of major histocompatibility complex genes in a rat model of Parkinson's disease. PLoS ONE 9: e91663.
- Grieb B, von Nicolai C, Engler G, Sharott A, Papageorgiou I, et al. (2013) Decomposition of abnormal free locomotor behavior in a rat model of Parkinson's disease. Front Syst Neurosci 7: 95.
- Zaidel A, Spivak A, Grieb B, Bergman H, Israel Z (2010) Subthalamic span of beta oscillations predicts deep brain stimulation efficacy for patients with Parkinson's disease. Brain 133: 2007–2021.

Eidesstattliche Versicherung

Ich versichere ausdrücklich, dass ich die Arbeit selbständig und ohne fremde Hilfe verfasst, andere als die von mir angegebenen Quellen und Hilfsmittel nicht benutzt und die aus den benutzten Werken wörtlich oder inhaltlich entnommenen Stellen einzeln nach Ausgabe (Auflage und Jahr des Erscheinens), Band und Seite des benutzten Werkes kenntlich gemacht habe.

Ferner versichere ich, dass ich die Dissertation bisher nicht einem Fachvertreter an einer anderen Hochschule zur Überprüfung vorgelegt oder mich anderweitig um Zulassung zur Promotion beworben habe.

Ich erkläre mich einverstanden, dass meine Dissertation vom Dekanat der Medizinischen Fakultät mit einer gängigen Software zur Erkennung von Plagiaten überprüft werden kann.

Unterschrift: